Available online at www.sciencedirect.com
ScienceDirect
Biochemical and Biophysical Research Communications 350 (2006) 82–90
BBRC
www.elsevier.com/locate/ybbrc

# Monoubiquitylation of GGA3 by hVPS18 regulates its ubiquitin-binding ability

Satomi Yogosawa [a,b], Masato Kawasaki [c], Soichi Wakatsuki [c], Eiki Kominami [d], Yoko Shiba [e], Kazuhisa Nakayama [e], Shinichi Kohsaka [a,*], Chihiro Akazawa [a]

[a] *Department of Neurochemistry, National Institute of Neuroscience, NCNP, Kodaira, Tokyo 187-8502, Japan*
[b] *Division of Molecular Biology, Research Institute for Biological Sciences, Tokyo University of Science, Noda, Chiba 278-0022, Japan*
[c] *Structural Biology Research Center, Photon Factory, Institute of Materials Structure Science, High Energy Accelerator Research Organization (KEK), Tsukuba, Ibaraki 305-0801, Japan*
[d] *Department of Biochemistry, Juntendo University School of Medicine, Bunkyo-ku, Tokyo 113-8421, Japan*
[e] *Graduate School of Pharmaceutical Science, Kyoto University, Sakyo-ku, Kyoto 606-8501, Japan*

Received 25 August 2006
Available online 15 September 2006

**Abstract**

GGAs (Golgi-localizing, γ-adaptin ear domain homology, ADP-ribosylation factor (ARF)-binding proteins), constitute a family of monomeric adaptor proteins and are associated with protein trafficking from the *trans*-Golgi network to endosomes. Here, we show that GGA3 is monoubiquitylated by a RING-H2 type-ubiquitin ligase hVPS18 (human homologue of *vacuolar protein sorting* 18). By *in vitro* ubiquitylation assays, we have identified lysine 258 in the GAT domain as a major ubiquitylation site that resides adjacent to the ubiquitin-binding site. The ubiquitylation is abolished by a mutation in either the GAT domain or ubiquitin that disrupts the GAT-ubiquitin interaction, indicating that the ubiquitin binding is a prerequisite for the ubiquitylation. Furthermore, the GAT domain ubiquitylated by hVPS18 no longer binds to ubiquitin, indicating that ubiquitylation negatively regulates the ubiquitin-binding ability of the GAT domain. These results suggest that the ubiquitin binding and ubiquitylation of GGA3-GAT domain are mutually inseparable through a ubiquitin ligase activity of hVPS18.


*Keywords:* GGA; GAT-domain; hVPS18; RING-H2 domain; Ubiquitin ligase; Monoubiquitylation; Ubiquitin-binding

In eukaryotic cells, vesicular trafficking of proteins between intracellular compartments, such as the Golgi complex and the multivesicular body (MVB)/lysosome, plays an important role in cellular functions. GGAs (Golgi-localizing, γ-adaptin ear domain homology, ADP-ribosylation factor (ARF)-binding proteins) are a family of monomeric adaptor proteins that regulate delivery of clathrin-coated vesicles from the TGN to endosomes [1–3]. In mammals, there are three GGAs (GGA1, GGA2, and GGA3) that share four functional domains, named VHS (Vps27/Hrs/Stam), GAT (GGA and Tom1 (target of Myb 1)), hinge, and GAE (γ-adaptin ear) [4–7]. The N-terminal VHS domain directly binds to acidic cluster-dileucine motifs found in the cytoplasmic domains of transmembrane cargo proteins [8–10]. The GAT domain is responsible for association of GGAs with the TGN membrane through interacting with activated ARF (a GTP-bound form) [11]. The proline-rich hinge region, the most variable among the GGA isoforms, mediates recruitment of clathrin [12]. The C-terminal GAE domain associates with various accessory proteins that modulate vesicle transport [1,3].

In the past few years, a number of proteins that are involved in membrane trafficking, especially in endocytosis and degradation in lysosomes, have been shown to be

* Corresponding author. Fax: +81 42 346 1751.
*E-mail address:* kohsaka@ncnp.go.jp (S. Kohsaka).

0006-291X/$ - see front matter © 2006 Elsevier Inc. All rights reserved.
doi:10.1016/j.bbrc.2006.09.013

functionally modulated by their ubiquitin binding and ubiquitylation [13–16]. Recently, it has also been shown that ubiquitin binding and ubiquitylation play an important role in selective transport of proteins from the TGN. The GAT domains of GGAs bind to ubiquitin and/or ubiquitylated proteins and undergo monoubiquitylation in the cell [17–20]. The interaction between the GAT domain and ubiquitin may endow GGAs with the ability to sort ubiquitylated transmembrane proteins at both the TGN and endosomes. Several ubiquitin ligases (E3) have been shown to be involved in monoubiquitylation of membrane-associated proteins and to participate in the endocytic and degradation pathways [21]. For example, c-Cbl, a RING-type ligase, ubiquitylates epidermal growth factor receptor (EGFR) depending on ligand-stimulated phosphorylation of the receptor [22], and Nedd4, a HECT-type ligase, is required for monoubiquitylation of eps15 and Hrs [23,24].

The Class C Vps (vacuolar protein sorting) complex is required for vesicle transport from the late endosome to vacuole in yeast [25,26]. In mammals, VPS proteins also appear to control the fusion events of late endosomes and lysosomes [27,28]. In humans, four Class C VPS proteins, hVPS11, hVPS16, hVPS18, and hVPS33, constitute a large hetero-oligomeric complex that interacts with syntaxin 7 at late endosomes/lysosomes [29]. Moreover, they also exist as a large detergent-insoluble HOPS (homotypic fusion and vacuole protein sorting) complex that contains additional components, hVPS39/Vam6, and hVPS41/Vam2 [27]. Overexpression of VPS39/Vam6S alters the late endosome function in mammalian cells [30]. Thus, it is necessary to discuss specific functions of Class C VPS proteins based on the biochemical properties.

In this report, we have demonstrated that GGAs (GGA1 and GGA3 but not GGA2) are monoubiquitylated by hVPS18, a RING-H2 type ubiquitin ligase, and identified a lysine residue in the C-terminal subdomain of the GAT domain as a major ubiquitylation site. Furthermore, we have shown that the monoubiquitylation negatively regulates the ubiquitin-binding ability of GGA itself. These observations shed light on the regulatory mechanisms of GGA to participate in membrane trafficking through the association of hVPS18.

## Materials and methods

*Plasmid construction.* Full-length and various truncated human GGA cDNAs, as described previous, [17], were subcloned into the following vector: the pGEX-4T2 (Amersham Biosciences) prokaryotic expression vector for the production of GST-tagged fusion proteins. Myc-tagged hVPS18 and hVPS11 mammalian expression vectors were prepared as described previously [29]. The full-length hVPS18, hVPS11, and hVPS16 were subcloned into pFastBacHTb insect expression vector (Invitrogen) to generate $His_6$-tagged fusion proteins.

*Expression and preparation of recombinant proteins.* E2 ubiquitin-conjugating enzyme, human Ubc4, was produced in *Escherichia coli* strain BL21-AI (Invitrogen). GST-GGA (wild-type and truncated mutants) and GST-ubiquitin (Ub) (wild-type and mutants) were expressed in *E. coli* strain BL21-AI and the recombinant proteins were purified by using glutathione–Sepharose 4B beads (Amersham Biosciences) in PBS containing 1 mM PMSF, Complete protease inhibitor mixture, and 1% Triton X-100. $His_6$-tagged hVPS18, hVPS11, and hVPS16 were expressed in Sf-9 insect cells using baculovirus protein expression system (Invitrogen) and the recombinant proteins were purified under the denatured condition (8 M urea), and followed by using TALON metal affinity beads (BD Biosciences), and renatured in PBS. Circular dichroism spectra of the wild-type and mutant proteins were recorded on a Jasco J-820 spectropolarimeter at 25 °C using a cuvette with 1 mm path length with the protein concentration of 30 μM in PBS.

*Antibody.* Polyclonal antibody against human GGA1, GGA2, and GGA3 was raised in rats by immunization with purified full-length GGA1, GGA2, and GGA3, respectively. These antibodies were affinity-purified on HiTrap NHS-activated columns (Amersham Biosciences) conjugated with immunogens. Monoclonal GGA3 antibody was purchased from BD Transduction Laboratories. Anti-hVPS18, hVPS11, and hVPS16 antibodies were prepared as described previously [29].

*Immunocytochemistry.* HeLa cells were immunostained with mouse anti-GGA3 antibody and rabbit anti-hVPS18 as described previously [29]. To confirm intracellular colocalization, immunoreactivities were analyzed by the sectioning microscope (Delta Vision) calibrated by using fluorescent beads (TetraSpeck Fluorescent Microsphere Standards, 0.1 μm, Invitrogen).

*Immunoprecipitation.* Immunoprecipitation was performed as described previously [29]. Briefly, the cells were transfected with various plasmids by Fugene 6 reagent (Roche Molecular Biochemicals) according to the manufacturer's instructions. At 24 h after transfection, total cell lysates were incubated with 4 μg of anti-FLAG antibodies (monoclonal M2, Sigma) at 4 °C overnight. Immunoprecipitation of the antigen-antibody complex was accomplished by adding 40 μl of protein G–Sepharose for 1 h at 4 °C. Sepharose bound proteins were subjected to SDS–PAGE and detected by Western blot analyses with anti-Myc antibody (Roche Molecular Biochemicals) or anti-FLAG M2 antibody, respectively.

*In vitro pull-down assay. In vitro* pull-down assay was performed as described previously [31]. Briefly, GST-GGA-GAT proteins were immobilized on glutathione–Sepharose 4B beads and incubated with $His_6$-hVPS18 at 25 °C for 30 min. The resin was washed, subjected to SDS–PAGE, and detected by Western blot analyses with either anti-$His_6$ antibody (Santa Cruz Biotechnology) or anti-GST antibody.

We performed assays of GGA3 binding to ubiquitin as described previous [17]. Briefly, various GGA3 proteins were incubated with Ub-(10 μl) or protein A–agarose (15 μl) beads (Sigma) for 1 h at room temperature. The beads were washed, subjected to SDS–PAGE, and detected by Western blot analyses using anti-GST antibody.

To prepare ubiquitylated GGA3 C-GAT proteins, GGA3 C-GAT proteins were subjected to *in vitro* ubiquitylation assay and immobilized on glutathione–Sepharose 4B beads. The beads were then washed with a buffer (25 mM Hepes, pH 7.4, 0.1% Nonidet P-40, 0.5 M NaCl, and 50% ethylene glycol) and eluted with 25 mM Hepes, pH 7.4, 20 mM reduced glutathione.

*In vitro ubiquitylation assay.* An *in vitro* ubiquitylation assay was performed as described previously [29]. Briefly, GST-GGA proteins were mixed with yeast E1 (500 ng) (Boston Biochem), human Ubc4, ubiquitin (Boston Biochem) or GST-Ub (10 or 5 μg, respectively), and $His_6$-tagged hVPS18 (or hVPS11 or hVPS16). The mixture was incubated at 25 °C for 30 or 60 min in the presence of 50 mM Tris–HCl, pH 7.4, 5 mM $MgCl_2$, 2 mM dithiothreitol (DTT), and 4 mM ATP in a 20 μl volume. After incubation, the mixtures were immobilized on glutathione–Sepharose 4B beads and washed with wash buffer for three times. The resin was subjected to SDS–PAGE and detected by Western blot analyses using anti-GST antibody or anti-$His_6$ antibody or specific antibody.

## Results and discussion

### *Direct interaction with GGAs and hVPS18*

Recent studies identified the GAT domain as a ubiquitin-binding module [17–20]. Furthermore, our recent yeast

two-hybrid screening using hVPS18 as bait identified a partial fragment of GGA3 [31]. We first confirmed the molecular interaction by an *in vitro* pull-down assay using recombinant GGAs and hVPS18. As shown in Fig. 1A, $His_6$-hVPS18 was pulled down with the GST fusion of the GAT domain of GGA1, GGA2 or GGA3. We next analyzed the *in vivo* interaction by a co-immunoprecipitation experiment using lysates of cells cotransfected with FLAG-GGAs and either Myc-hVPS18 or Myc-hVPS11. As shown in Fig. 1B, all GGAs co-immunoprecipitated hVPS18. By contrast, either GGA could not interact with hVPS11, another Class C component having a RING-H2

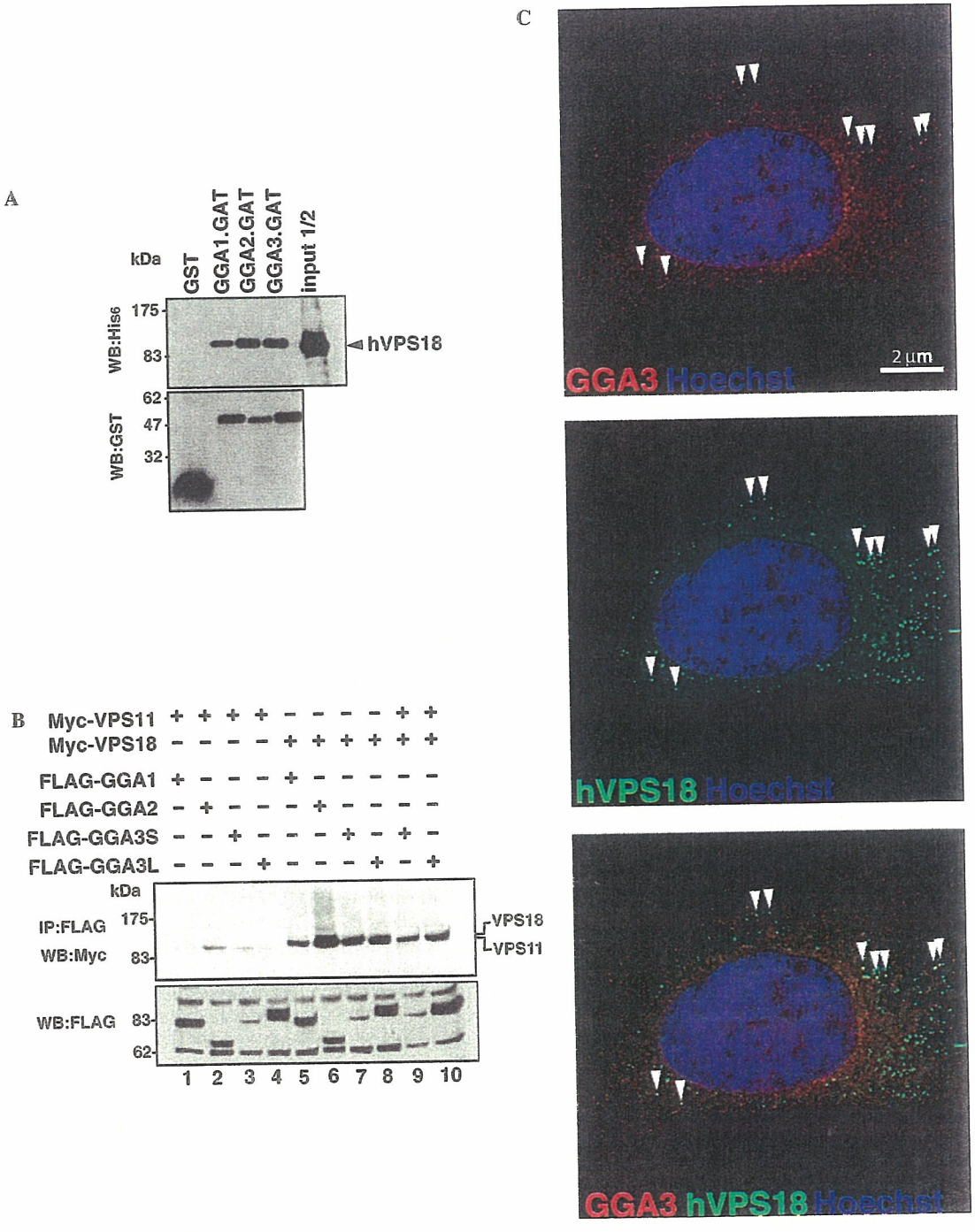


Fig. 1. GGA-GAT domains interact with hVPS18. (A) $His_6$-hVPS18 bound to three GST-GGA-GAT proteins was detected by Western blot analyses using anti-GST antibody. (B) Cos7 cells were co-transfected with $His_6$-FLAG-GGAs and Myc-hVPS11 or hVPS18. At 24 h post-transfection, whole-cell lysates were co-immunoprecipitated using anti-FLAG M2 antibody. Immunoprecipitates were resolved by SDS–PAGE and detected by Western blot analyses using indicated antibody. (C) The interaction of endogenous GGA3 (*Red*) and hVPS18 (*Green*) in HeLa cells was detected by immunocytochemistry. Colocalizing profiles are pointed out with *arrows*. *Bar*, 2 μm.

domain. Considering the molecular interaction between GGAs and hVPS18, a major issue that arises is the intracellular localization of these proteins. GGAs have been characterized as TGN-associated clathrin adaptors, whereas the Class C VPS complex has been proposed to function in endosomal/lysosomal compartments. We therefore analyzed the precise intracellular localization of endogenous GGA3 and hVPS18 in HeLa cells by the sectioning microscopy. The optical pathways were calibrated using fluorescent labeled beads (0.1 μm diameter). The thirty series of sections covering 5 μm thickness were captured and deconvoluted images were analyzed. As shown in a representative image Fig. 1C, GGA3 immunoreactivities (colored in *Red*) and hVPS18 immunoreactivities (colored in *Green*) were often colocalized on punctuates (colored in *Yellows*) of perinuclear structures (indicated by arrowheads).

### *Monoubiquitylation of GGAs by hVPS18, RING-H2 type ubiquitin ligase*

Our recent study, showed that the RING-H2 domain of hVPS18 displays a E3 ubiquitin ligase activity [31]. To examine whether GGAs are ubiquitylated by the hVPS18, we performed an *in vitro* ubiquitylation assay using full-length GGAs as substrates. As shown in Fig. 2A, the molecular weight of GGA1 and GGA3 was shifted by ~8 kDa only in the simultaneous presence of ubiquitin, E1, E2 (UbcH4), and hVPS18 (lanes 2 and 6, respectively). By contrast, the shift was not observed in the case of GGA2 (lane 4), being compatible with our previous study showing that GGA2 is not able to interact with ubiquitin nor ubiquitylated in the cell. We next examined whether the *in vitro* modification represents monoubiquitylation/multiubiquitylation or not. In this experiment, we used wild-type (WT) ubiquitin fused to GST, and its K48R and KO (all lysine residues were replaced with arginine) mutants, since these mutants are not conjugated to conventional polyubiquitin chains. As shown in Fig. 2B, when GST-ubiquitin WT was used, the molecular weight of the GGA3-GAT domain was shifted by 35 kDa, which corresponds to the size of GST-ubiquitin. Essentially the same band shift was observed using the K48R and KO mutants, indicating that GGA3 is mainly monoubiquitylated by hVPS18.

Since hVPS18 forms a complex with other Class C VPS components [29], we then examined whether hVPS11 and hVPS16 were also involved in the monoubiquitylation of GGA3. Although hVPS11 also has a RING-H2 domain and shows a ubiquitin ligase activity (data not shown), it did not ubiquitylate the GGA3-VHS+GAT domain irrespective of the presence of hVPS16 (Fig. 2C lanes 2 and 3). However, the monoubiquitylation of GGA3 by hVPS18 was extremely enhanced in the presence of hVPS11 and hVPS16 (compare lane 5 with lanes 6 and 7). This result makes it likely that hVPS18 is involved in the monoubiquitylation of GGA3 as a Class C VPS complex.

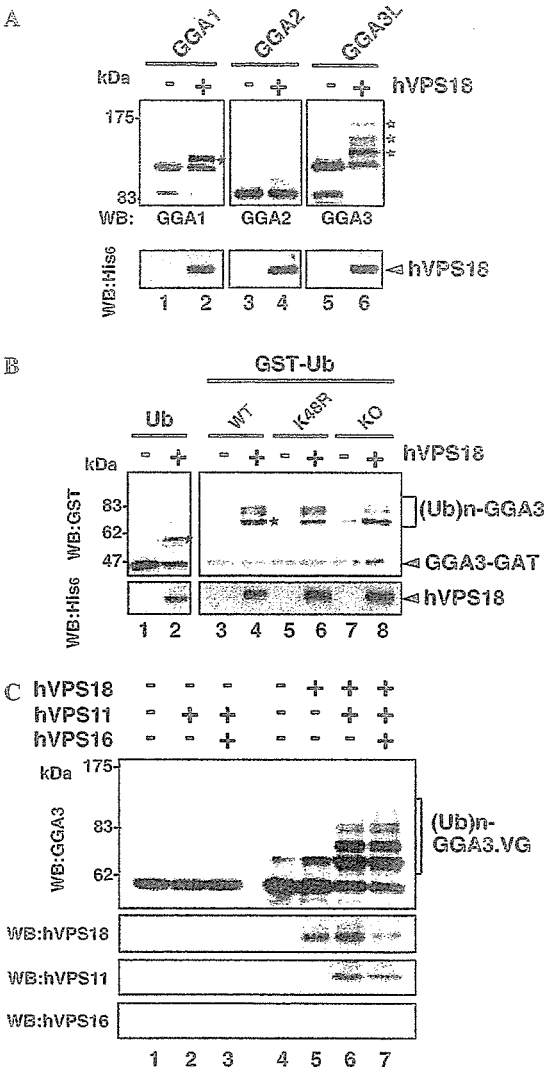


Fig. 2. GGAs are monoubiquitylated by hVPS18. (A) The *in vitro* ubiquitylation of GST-GGAs wild-type by $His_6$-hVPS18. The sample was detected by Western blot analyses using anti-GGA1, GGA2, or GGA3 (upper panel). Purified $His_6$-hVPS18 protein was detected by Western blot analyses using anti-$His_6$ antibody (lower panel). Asterisks represent ubiquitylated form of GGAs. (B) The *in vitro* ubiquitylation of GST-GGA3-GAT protein in the presence of no-tagged ubiquitin (Ub) or GST-fused ubiquitin (GST-Ub); wild-type (WT), K48R, or all lysines mutated to arginines (KO). The sample was detected by Western blot analyses using anti-GST or anti-$His_6$ antibody. Asterisks represent ubiquitylated forms of GGA3 that conjugate to Ub (left panel) or GST-Ub (right panel). (C) The *in vitro* ubiquitylation of GST-GGA3-VG (VHS+GAT) by hVPS11 or hVPS18 in the presence or absence of hVPS16. Purified $His_6$-tagged hVPS18 (or hVPS11 or hVPS16) protein was detected by Western blot analyses using specific antibodies.

### *Ubiquitin binding-dependent monoubiquitylation of GGA3-GAT*

Identification of the ubiquitylation site is of great significance to discuss the molecular mechanism underlying the GGA ubiquitylation. We have recently shown that GGA3 is ubiquitylated in the C-terminal subdomain of its GAT domain (C-GAT) *in vivo* [17]. We therefore,

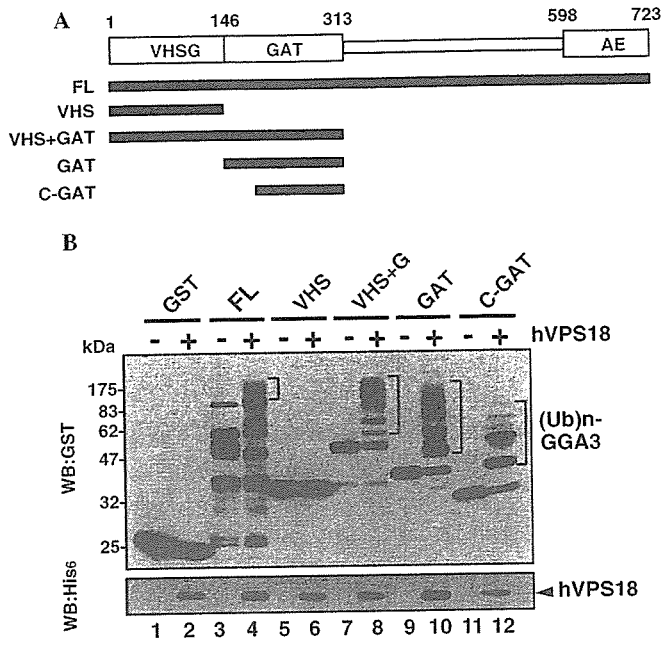


Fig. 3. GGA3 is ubiquitylated in the C-GAT domain. (A) Schematic representation of GGA3. (B) The *in vitro* ubiquitylation of GST-GGA3 full-length or truncated mutants. The sample was detected by Western blot analyses using anti-GST or anti-$His_6$ antibody. The positions of ubiquitylated GGA3 are indicated by a bracket.

performed an *in vitro* ubiquitylation assay using various truncation mutants of GGA3 (Fig. 3A). As shown in Fig. 3B, ubiquitylation occurred in the GGA3 fragments covering the C-GAT subdomain (lanes 4, 8, 10, and 12) but not in the GST protein (lane 2) nor the VHS domain alone (lane 6), in agreement with our previous ubiquitylation data in the cell [17].

Recent studies have shown, that many proteins containing ubiquitin-binding modules undergo monoubiquitylation and more importantly, their ubiquitin-binding ability is required for their own monoubuquitylation [23,32,33]. Therefore, we tested *in vitro* whether various GGA3 mutants that lack ubiquitin-binding ability were monoubiquitylated by hVPS18. As shown in Supplementary Fig. 1, the GGA3-GAT helix α3 mutant (L280R or D284G) defective in ubiquitin binding was not monoubiquitylated (compare lane 2 with lanes 6 and 8). Essentially the same result was obtained with a GGA3-GAT helix α2/α3 double mutant, E250N/D284G. These results indicate that binding to ubiquitin is a prerequisite for the GGA3 ubiquitylation. Next we constructed various truncated mutants of the GGA3-GAT domain (Supplementary Fig. 2A) and compared their ubiquitin binding (in Supplementary Fig. 2B) and ubiquitylation by hVPS18 (Supplementary Fig. 2C). Remarkably, all of the GAT fragments that retained ubiquitin-binding ability were monoubiquitylated by hVPS18, whereas the fragments lacking the ability were not monoubiquitylated. These data indicate that binding to ubiquitin and ubiquitylation of the GAT domain are intimately coupled events.

### *Lys258 is the major ubiquitylation site*

In the C-GAT subdomain of GGA3, there are six lysine residues that can be conjugated to ubiquitin. To determine which lysine residue(s) was ubiquitylated, we systematically replaced the lysine residues with arginines (Fig. 4A) and examined binding to ubiquitin and monoubiquitylation of these lysine mutants. As shown in Fig. 4B, all of the C-GAT mutants examined retained their ubiquitin-binding ability. In striking contrast, they were variable in the ubiquitylation efficiency (Fig. 4C). Namely, (i) a mutant, 5KR(258), in which all the lysine residues except for K258 were replaced with arginines (Fig. 4A), underwent monoubiquitylation (lane 10) at comparable efficiency to that of the WT C-GAT subdomain (lane 2); (ii) the 5KR(249), 5KR(264), and 5KR(294) mutants underwent ubiquitylation at extremely low efficiency (lanes 8, 12, and 14); and (iii) ubiquitylation of 5KR(210), 5KR(213), and 6KR mutants was under the detection level (lanes 4, 6, and 16). As shown in Supplemental Figure 4, the circular dichroism spectra of WT and 5KR(258) were almost identical, suggesting that the mutations did not significantly affect the overall conformation of the C-GAT subdomain. Taken together, we conclude that lysine 258 is the major site ubiquitylated by hVPS18, although other lysine residues at positions 249, 264, and 294 were also ubiquitylated to some extent.

### *Model of GGA3-GAT domain ubiquitylated at Lys258*

Previously, we determined the crystal structure of the complex between GGA3 C-GAT and ubiquitin, and showed primarily hydrophobic interactions in which the site 1 in C-CAT constitutes the binding site with three times higher affinity than the site 2 [34]. To understand the molecular basis for the coupling of ubiquitin binding and ubiquitylation of the GGA3-GAT domain, we mapped the positions of lysine residues of GGA3 C-GAT in the complex structure (Fig. 5). Among the six candidate lysine residues, lysine 258 is the closest to the C-terminus of ubiquitin (Fig. 5, Table 1), suggesting that this lysine is most susceptible to ubiquitin conjugation. This model also suggests that no major structural rearrangement between ubiquitin and the GGA3 C-GAT domain is required for the ubiquitylation of lysine 258.

### *Ubiquitylated GGA3 C-GAT loses its ubiquitin-binding ability*

Hicke et al. have proposed a possibility that ubiquitylation of ubiquitin-binding proteins might generally have a regulatory function by affecting association of their ubiquitin-binding modules with either free ubiquitin or ubiquitylated proteins [13]. To address this possibility, we performed *in vitro* pull-down assay using reaction products of the *in vitro* ubiquitylation, in which both ubiquitylated and non-ubiquitylated C-GAT proteins were included. As

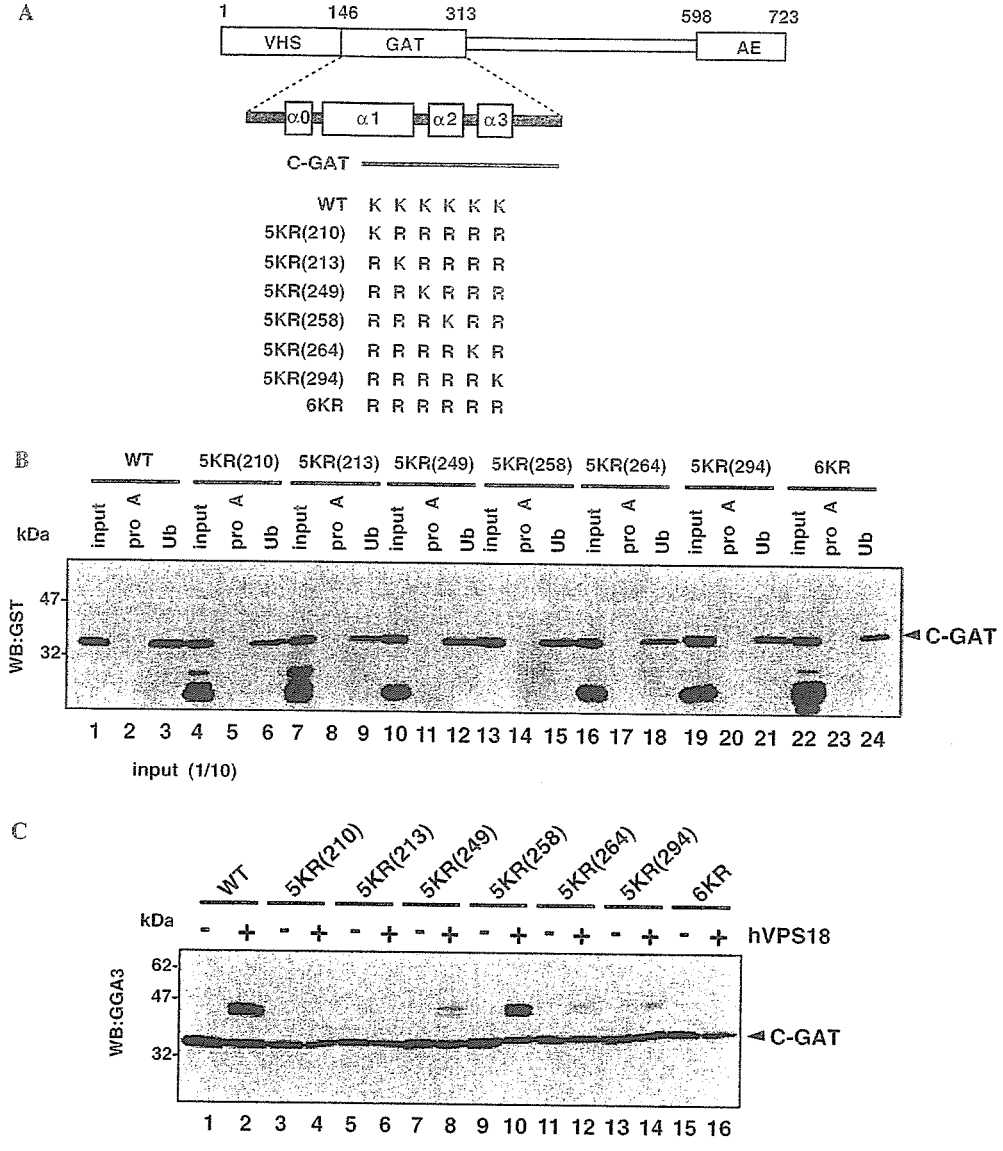


Fig. 4. GGA3 is mainly ubiquitylated at lysine 258 that resides in the two ubiquitin-binding sites. (A) Schematic representation of GGA3-GAT. (B) The *in vitro* pull-down assay of GGA3 C-GAT. Equal amounts of purified GGA3 C-GAT proteins were incubated with Ub- or Protein-A–agarose. The resin was washed, subjected to SDS–PAGE, and detected by Western blot analyses with anti-GST antibody. Ten percent of input samples were loaded on *input lanes*. (C) The *in vitro* ubiquitylation of GST-GGA3 C-GAT proteins. The sample was detected by Western blot analyses using anti-GGA3 antibody.

shown in Fig. 6, the ubiquitylated form of C-GAT WT or its 5KR(258) mutant was not pulled down with ubiquitin-agarose beads (lanes 3 and 7, indicated by asterisks), whereas their non-ubiquitylated forms were pulled down well. This result indicates that covalent modification by ubiquitin at lysine 258 makes C-GAT inaccessible to ubiquitin.

Recent advances have uncovered that several membrane-trafficking events are mediated by ubiquitin binding and monoubiquitylation, including changes in subcellular localization, protein conformation, activity, and protein-protein interaction. [16,35,36]. GGA might have evolved to allow a wide variety of proteins to interact directly with ubiquitin or ubiquitylated proteins during various cellular processes [1,20,37,38]. In this study, we first identified that hVPS18 acts as a genuine ubiquitin ligase of GGAs (Fig. 2A). The modification by hVPS18 slightly differs among GGAs; the monoubiquitylation occurs in one or multiple lysine sites of GGA1 and GGA3 but not of GGA2 (Figs. 2A and B). We then focused on GGA3 and tried to identify the responsible lysine. By taking an advantage of E3 identification, we utilized various KR mutants (Fig. 4). Finally, we identified the lysine 258 is the main target lysine for the ubiquitylation by hVPS18. If we closely look at the results of co-crystallization of GGA3 C-GAT and ubiquitin, the lysine 258 is located at the closest position to the C-terminus of ubiquitin, suggesting that the ubiquitin binding is necessary for ubiquitylation.

It has been recently shown that a free ubiquitin or ubiquitylated proteins are recognized by small (20–150 amino

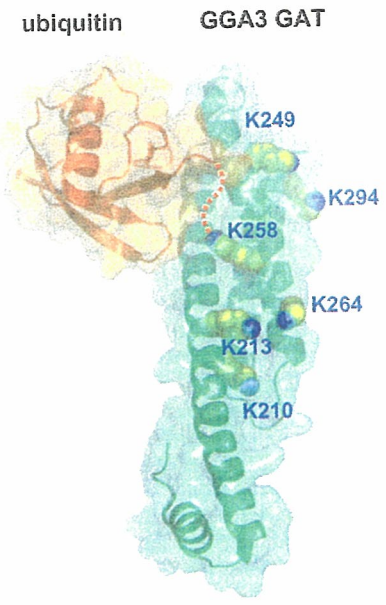


Fig. 5. Molecular surface representation of GGA3 C-GAT. The model was built by combining the crystal structures of the complex between ubiquitin and GGA3 C-GAT subdomain [34] and the entire GGA1 GAT domain [44]. Ubiquitin and GGA3 GAT domain are shown as ribbon diagrams with transparent surface representations (ubiquitin, *Orange*; GGA3 GAT, *Green*). Six lysine residues of the GGA3 C-GAT subdomain are shown with space-filling atoms (carbon atoms, *Yellow*; nitrogen atoms, blue). The C-terminal of ubiquitin (The last visible residue in the crystal, Leu73) and the side chain of Lys258 of GGA3 GAT are connected by an orange dotted line. Figure was drawn using PyMOL (http://pymol.sourceforge.net).

Table 1
Distances between the nitrogen atoms of the lysine side chains of C-GAT and the α carbon atom of Leu73 of ubiquitin, in the model structure in Fig. 5

| *Lysine* | *210* | *213* | *249* | *258* | *264* | *294* |
|---|---|---|---|---|---|---|
| Distance (Å) | 32.0 | 24.1 | 14.3 | 12.7 | 24.5 | 21.5 |

Leu73 of ubiquitin is the C-terminal residue visible in the crystal.

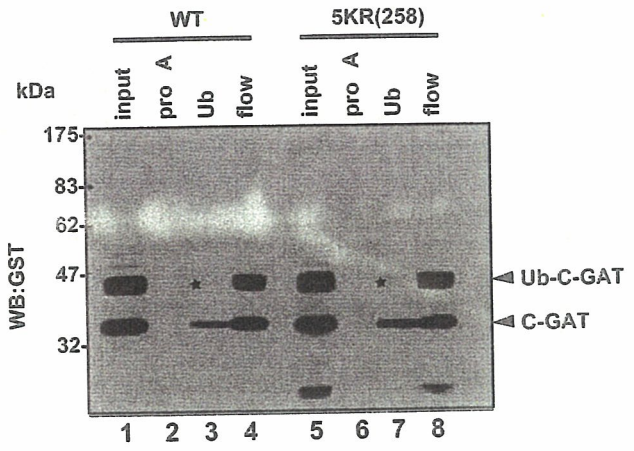


Fig. 6. Ubiquitylated GGA3 prevents further attachment to ubiquitin. The *in vitro* pull-down assay of ubiquitylated GGA3-GAT proteins. Equal amounts of ubiquitylated GGA3-GAT proteins were incubated with Ub- or Protein-A–agarose. The resin was washed, subjected to SDS–PAGE, and detected by Western blot analyses with anti-GST antibody. The supernatants were subjected to incubate with glutathione–Sepharose 4B (lanes 4 and 8). The 25% of input samples were loaded on *input lanes* (lane 1 and 5). Asterisks indicate that ubiquitylated forms of GGA3-GAT could not bind to Ub-agarose.

acids), independently folded motifs; ubiquitin-interacting motif (UIM), ubiquitin-associated (UBA), ubiquitin-conjugating enzyme-like (UBC)/ubiquitin E2 variant (UEV), or Cue1-homologous (CUE) domains [39]. These domains are also referred to as ubiquitin receptors [40]. However, in most cases, little is understood how biochemical interactions are transferred to downstream signals by these ubiquitin-binding proteins. Immediately after ubiquitin-binding abilities were reported, it was generally accepted that ubiquitin receptors are themselves ubiquitylated. Interestingly, the ubiquitylation of ubiquitin receptors requires ubiquitin binding. From our results, all of the GAT mutants that lack ubiquitin binding also inhibit ubiquitylation (Fig. 6). Conversely, a ubiquitin mutant (Ile44Ala) that cannot bind ubiquitin receptors per se cannot be conjugated to GAT domain. Previous reports described that the GAT domain contains two binding sites for ubiquitin [34]. The site 1 centers on leucine 227 and the site 2 centers on leucine 276. The site 1 has a higher affinity for ubiquitin than does site 2. When a ubiquitin was conjugated to the lysine 258 that is close to the site 1, no more ubiquitin can bind to the GGA3 C-GAT. This type of autoinhibition is reminiscent of intramolecular SH2-domain-phosphotyrosine interaction [41]. There has been a strong link between the presence of ubiquitin binding in a protein and its ubiquitylation. Ubiquitin binding and ubiquitylation of ubiquitin receptors are closely coupled and mutually inseparable [42,43]. But so far no ubiquitylation of lysine in the UBD has been reported. This is the first example demonstrating the ubiquitylated lysine resides in the UBD and consequently inhibit further ubiquitin binding. hVPS18 is one of the responsible E3 ubiquitin ligases that directly regulate the ubiquitin binding by conjugating ubiquitin in UBD of GGA3. A major question that has not been answered is to test how E3 hVPS18 is recruited to ubiquitin-binding proteins.

The ubiquitin ligase E3 functions as a monomer or a complex with other cofactors, such as SCF (Skp1/cullin/F-box protein) and the anaphase-promoting complex or cyclosome (APC/C) [35]. But none of the ligase activity has been observed when the catalytic subunit was solely added. Our study showed hVPS18, in the presence of E1 and E2, is sufficient for the *in vitro* ubiquitylation of GGA3, but the modification was significantly enhanced when equal molar of hVPS11 and hVPS16 are mixed. Previous report demonstrated that hVPS18, hVPS11, and hVPS16 constitute a hetero-oligomeric complex in the cytosolic membrane of endosome/lysosome [29]. The aug-

mented ligase-activity implies that the complex formation plays the functionally significant role both *in vivo* and *in vitro*.

In this report, we identified hVPS18 as a ubiquitin ligase (E3) for the monoubiquitylation of GGAs through their ability of ubiquitin-interaction. A number of molecules have been reported to interact with GGA, such as ARF, Rabaptin-5, clathrin, AP-1, and γ-synergin [1,3]. It will be a next issue to address whether these interactions are regulated via monoubiquitylation by hVPS18.

## Appendix A. Supplementary data

Supplementary data associated with this article can be found, in the online version, at doi:10.1016/j.bbrc.2006.09.013.

## References

[1] J.S. Bonifacino, The GGA proteins: adaptors on the move, Nat. Rev. Mol. Cell. Biol. 5 (2004) 23–32.
[2] I. Hinners, S.A. Tooze, Changing directions: clathrin-mediated transport between the Golgi and endosomes, J. Cell Sci. 116 (2003) 763–771.
[3] K. Nakayama, S. Wakatsuki, The structure and function of GGAs, the traffic controllers at the TGN sorting crossroads, Cell Struct. Funct. 28 (2003) 431–442.
[4] E.C. Dell'Angelica, R. Puertollano, C. Mullins, R.C. Aguilar, J.D. Vargas, L.M. Hartnell, J.S. Bonifacino, GGAs: a family of ADP ribosylation factor-binding proteins related to adaptors and associated with the Golgi complex, J. Cell Biol. 149 (2000) 81–94.
[5] H. Takatsu, K. Yoshino, K. Nakayama, Adaptor gamma ear homology domain conserved in gamma-adaptin and GGA proteins that interact with gamma-synergin, Biochem. Biophys. Res. Commun. 271 (2000) 719–725.
[6] J. Hirst, W.W. Lui, N.A. Bright, N. Totty, M.N. Seaman, M.S. Robinson, A family of proteins with gamma-adaptin and VHS domains that facilitate trafficking between the trans-Golgi network and the vacuole/lysosome, J. Cell Biol. 149 (2000) 67–80.
[7] M. Kawasaki, K. Nakayama, S. Wakatsuki, Membrane recruitment of effector proteins by Arf and Rab GTPases, Curr. Opin. Struct. Biol. (2005).
[8] R. Puertollano, R.C. Aguilar, I. Gorshkova, R.J. Crouch, J.S. Bonifacino, Sorting of mannose 6-phosphate receptors mediated by the GGAs, Science 292 (2001) 1712–1716.
[9] Y. Zhu, B. Doray, A. Poussu, V.P. Lehto, S. Kornfeld, Binding of GGA2 to the lysosomal enzyme sorting motif of the mannose 6-phosphate receptor, Science 292 (2001) 1716–1718.
[10] H. Takatsu, Y. Katoh, Y. Shiba, K. Nakayama, Golgi-localizing, gamma-adaptin ear homology domain, ADP-ribosylation factor-binding (GGA) proteins interact with acidic dileucine sequences within the cytoplasmic domains of sorting receptors through their Vps27p/Hrs/STAM (VHS) domains, J. Biol. Chem. 276 (2001) 28541–28545.
[11] H. Takatsu, K. Yoshino, K. Toda, K. Nakayama, GGA proteins associate with Golgi membranes through interaction between their GGAH domains and ADP-ribosylation factors, Biochem. J. 365 (2002) 369–378.
[12] R. Puertollano, P.A. Randazzo, J.F. Presley, L.M. Hartnell, J.S. Bonifacino, The GGAs promote ARF-dependent recruitment of clathrin to the TGN, Cell 105 (2001) 93–102.
[13] L. Hicke, H.L. Schubert, C.P. Hill, Ubiquitin-binding domains, Nat. Rev. Mol. Cell. Biol. 6 (2005) 610–621.
[14] M.D. Marmor, Y. Yarden, Role of protein ubiquitylation in regulating endocytosis of receptor tyrosine kinases, Oncogene 23 (2004) 2057–2070.
[15] P.P. Di Fiore, S. Polo, K. Hofmann, When ubiquitin meets ubiquitin receptors: a signalling connection, Nat. Rev. Mol. Cell. Biol. 4 (2003) 491–497.
[16] D.J. Katzmann, G. Odorizzi, S.D. Emr, Receptor downregulation and multivesicular-body sorting, Nat. Rev. Mol. Cell. Biol. 3 (2002) 893–905.
[17] Y. Shiba, Y. Katoh, T. Shiba, K. Yoshino, H. Takatsu, H. Kobayashi, H.W. Shin, S. Wakatsuki, K. Nakayama, GAT (GGA and Tom1) domain responsible for ubiquitin binding and ubiquitination, J. Biol. Chem. 279 (2004) 7105–7111.
[18] R. Puertollano, J.S. Bonifacino, Interactions of GGA3 with the ubiquitin sorting machinery, Nat. Cell Biol. 6 (2004) 244–251.
[19] P.M. Scott, P.S. Bilodeau, O. Zhdankina, S.C. Winistorfer, M.J. Hauglund, M.M. Allaman, W.R. Kearney, A.D. Robertson, A.L. Boman, R.C. Piper, GGA proteins bind ubiquitin to facilitate sorting at the trans-Golgi network, Nat. Cell Biol. 6 (2004) 252–259.
[20] R. Mattera, R. Puertollano, W.J. Smith, J.S. Bonifacino, The trihelical bundle subdomain of the GGA proteins interacts with multiple partners through overlapping but distinct sites, J. Biol. Chem. 279 (2004) 31409–31418.
[21] A. d'Azzo, A. Bongiovanni, T. Nastasi, E3 ubiquitin ligases as regulators of membrane protein trafficking and degradation, Traffic 6 (2005) 429–441.
[22] A.A. de Melker, G. van der Horst, J. Calafat, H. Jansen, J. Borst, c-Cbl ubiquitinates the EGF receptor at the plasma membrane and remains receptor associated throughout the endocytic route, J. Cell Sci. 114 (2001) 2167–2178.
[23] S. Polo, S. Sigismund, M. Faretta, M. Guidi, M.R. Capua, G. Bossi, H. Chen, P. De Camilli, P.P. Di Fiore, A single motif responsible for ubiquitin recognition and monoubiquitination in endocytic proteins, Nature 416 (2002) 451–455.
[24] M. Katz, K. Shtiegman, P. Tal-Or, L. Yakir, Y. Mosesson, D. Harari, Y. Machluf, H. Asao, T. Jovin, K. Sugamura, Y. Yarden, Ligand-independent degradation of epidermal growth factor receptor involves receptor ubiquitylation and Hgs, an adaptor whose ubiquitin-interacting motif targets ubiquitylation by Nedd4, Traffic 3 (2002) 740–751.
[25] T.K. Sato, P. Rehling, M.R. Peterson, S.D. Emr, Class C Vps protein complex regulates vacuolar SNARE pairing and is required for vesicle docking/fusion, Mol. Cell 6 (2000) 661–671.
[26] M.R. Peterson, S.D. Emr, The class C Vps complex functions at multiple stages of the vacuolar transport pathway, Traffic 2 (2001) 476–486.
[27] V. Poupon, A. Stewart, S.R. Gray, R.C. Piper, J.P. Luzio, The role of mVps18p in clustering, fusion, and intracellular localization of late endocytic prganelles, Mol. Bio. Cell 14 (2003) 4015–4027.
[28] S.C. Richardson, S.C. Winistorfer, V. Poupon, J.P. Luzio, R.C. Piper, Mammalian late vacuole protein sorting orthologues participate in early endosomal fusion and interact with the cytoskeleton, Mol. Biol. Cell 15 (2004) 1197–1210.
[29] B.Y. Kim, H. Kramer, A. Yamamoto, E. Kominami, S. Kohsaka, C. Akazawa, Molecular characterization of mammalian homologues of class C Vps proteins that interact with syntaxin-7, J. Biol. Chem. 276 (2001) 29393–29402.
[30] S. Caplan, L.M. Hartnell, R.C. Aguilar, N. Naslavsky, J.S. Bonifacino, Human Vam6p promotes lysosome clustering and fusion in vivo, J. Cell Biol. 154 (2001) 109–122.
[31] S. Yogosawa, S. Hatakeyama, K.I. Nakayama, H. Miyoshi, S. Kohsaka, C. Akazawa, Ubiquitylation and degradation of polo-like kinase SNK by hVPS18, a RING-H2 type ubiquitin ligase, J. Biol. Chem. 280 (2005) 41619–41627.
[32] S.L. Miller, E. Malotky, J.P. O'Bryan, Analysis of the role of ubiquitin-interacting motifs in ubiquitin binding and ubiquitylation, J. Biol. Chem. 279 (2004) 33528–33537.

[33] S.C. Shih, G. Prag, S.A. Francis, M.A. Sutanto, J.H. Hurley, L. Hicke, A ubiquitin-binding motif required for intramolecular monoubiquitylation, the CUE domain, EMBO J. 22 (2003) 1273–1281.
[34] M. Kawasaki, T. Shiba, Y. Shiba, Y. Yamaguchi, N. Matsugaki, N. Igarashi, M. Suzuki, R. Kato, K. Kato, K. Nakayama, S. Wakatsuki, Molecular mechanism of ubiquitin recognition by GGA3 GAT domain, Genes Cells 10 (2005) 639–654.
[35] A.M. Weissman, Themes and variations on ubiquitylation, Nat. Rev. Mol. Cell. Biol. 2 (2001) 169–178.
[36] R.C. Aguilar, B. Wendland, Ubiquitin: not just for proteasomes anymore, Curr. Opin. Cell Biol. 15 (2003) 184–190.
[37] Y. Katoh, Y. Shiba, H. Mitsuhashi, Y. Yanagida, H. Takatsu, K. Nakayama, Tollip and Tom1 form a complex and recruit ubiquitin-conjugated proteins onto early endosomes, J. Biol. Chem. 279 (2004) 24435–24443.
[38] M. Yamakami, T. Yoshimori, H. Yokosawa, Tom1, a VHS domain-containing protein, interacts with tollip, ubiquitin, and clathrin, J. Biol. Chem. 278 (2003) 52865–52872.
[39] K. Haglund, I. Dikic, Ubiquitylation and cell signaling, EMBO J. 24 (2005) 3353–3359.
[40] K. Haglund, P.P. Di Fiore, I. Dikic, Distinct monoubiquitin signals in receptor endocytosis, Trends Biochem. Sci. 28 (2003) 598–603.
[41] J. Kuriyan, D. Cowburn, Modular peptide recognition domains in eukaryotic signaling, Annu. Rev. Biophys. Biomol. Struct. 26 (1997) 259–288.
[42] M. Bienko, C.M. Green, N. Crosetto, F. Rudolf, G. Zapart, B. Coull, P. Kannouche, G. Wider, M. Peter, A.R. Lehmann, K. Hofmann, I. Dikic, Ubiquitin-binding domains in Y-family polymerases regulate translesion synthesis, Science 310 (2005) 1821–1824.
[43] D. Hoeller, N. Crosetto, B. Blagoev, C. Raiborg, R. Tikkanen, S. Wagner, K. Kowanetz, R. Breitling, M. Mann, H. Stenmark, I. Dikic, Regulation of ubiquitin-binding proteins by monoubiquitination, Nat. Cell Biol. 8 (2006) 163–169.
[44] T. Shiba, M. Kawasaki, H. Takatsu, T. Nogi, N. Matsugaki, N. Igarashi, M. Suzuki, R. Kato, K. Nakayama, S. Wakatsuki, Molecular mechanism of membrane recruitment of GGA by ARF in lysosomal protein transport, Nat. Struct. Biol. 10 (2003) 386–393.

American Journal of Pathology, Vol. 169, No. 1, July 2006

DOI: 10.2353/ajpath.2006.060085

*Cell Injury, Repair, Aging and Apoptosis*

# Photoreceptor Cell Apoptosis in the Retinal Degeneration of *Uchl3*-Deficient Mice

Yae Sano,*† Akiko Furuta,* Rieko Setsuie,*† Hisae Kikuchi,* Yu-Lai Wang,* Mikako Sakurai,*† Jungkee Kwon,*‡ Mami Noda,† and Keiji Wada*

*From the Department of Degenerative Neurological Diseases,* National Institute of Neuroscience, National Center of Neurology and Psychiatry, Tokyo, Japan; the Laboratory of Pathophysiology,† Graduate School of Pharmaceutical Sciences, Kyushu University, Fukuoka, Japan; and the Laboratory of Animal Medicine,‡ College of Veterinary Medicine, Chonbuk National University, Jeonju, Korea*

**UCH-L3 belongs to the ubiquitin C-terminal hydrolase family that deubiquitinates ubiquitin-protein conjugates in the ubiquitin-proteasome system. A murine *Uchl3* deletion mutant displays retinal degeneration, muscular degeneration, and mild growth retardation. To elucidate the function of UCH-L3, we investigated histopathological changes and expression of apoptosis- and oxidative stress-related proteins during retinal degeneration. In the normal retina, UCH-L3 was enriched in the photoreceptor inner segment that contains abundant mitochondria. Although the retina of *Uchl3*-deficient mice showed no significant morphological abnormalities during retinal development, prominent retinal degeneration became manifested after 3 weeks of age associated with photoreceptor cell apoptosis. Ultrastructurally, a decreased area of mitochondrial cristae and vacuolar changes were observed in the degenerated inner segment. Increased immunoreactivities for manganese superoxide dismutase, cytochrome *c* oxidase I, and apoptosis-inducing factor in the inner segment indicated mitochondrial oxidative stress. Expression of cytochrome c, caspase-1, and cleaved caspase-3 did not differ between wild-type and mutant mice; however, immunoreactivity for endonuclease G was found in the photoreceptor nuclei in the mutant retina. Hence, loss of UCH-L3 leads to mitochondrial oxidative stress-related photoreceptor cell apoptosis in a caspase-independent manner. Thus, *Uchl3*-deficient mice represent a model for adult-onset retinal degeneration associated with mitochondrial impairment.** *(Am J Pathol 2006, 169:132–141; DOI: 10.2353/ajpath.2006.060085)*

The ubiquitin system has been implicated in numerous cellular processes, including protein quality control, cell cycle, cell proliferation, signal transduction, membrane protein internalization, and apoptosis.[1,2] Ubiquitin-dependent processes are regulated by ubiquitinating enzymes, E1, E2, and E3, and deubiquitinating enzymes such as ubiquitin-specific proteases and ubiquitin C-terminal hydrolases (UCHs).[1,3–5] To date, four isozymes of UCHs, UCH-L1, UCH-L3, UCH-L4, and UCH-L5, have been cloned in mouse or human.[6–8] UCH-L1, also known as PGP 9.5, has been well characterized among the isozymes. UCH-L1 is selectively localized to brains and testis/ovaries[7] and functions as a ubiquitin ligase in addition to a deubiquitinating enzyme.[9] Furthermore, two distinct mutations are linked to Parkinson's disease in human[10] and gracile axonal dystrophy (*gad*) in mice.[11] UCH-L3, on the other hand, displays 52% amino acid identity to UCH-L1.[12] Uchl3 mRNA is expressed throughout various tissues and is especially enriched in testis and thymus.[13] In addition to its ubiquitin hydrolase activity, *in vitro* studies indicate that UCH-L3 cleaves the C terminus of the ubiquitin-like protein Nedd-8.[14,15] Although UCH-L1 and UCH-L3 are suggested to function as reciprocal modulators of germ cell apoptosis in experimental cryptorchid testis,[16] the cellular localization and function of UCH-L3 remain unknown in other organs.

Recently, *Uchl3*-deficient mice were generated with a deletion of exons 3 to 7, which are essential for hydrolase

Supported by grants-in-aid for scientific research from the Japan Society for the Promotion of Science; for priority area research from the Ministry of Education, Culture, Sports, Science and Technology, Japan; Kyushu University Foundation for Scientific Research from the Ministry of Health, Labour and Welfare, Japan; and the program for Promotion of Fundamental Studies in Health Sciences from the National Institute of Biomedical Innovation, Japan.

Accepted for publication March 23, 2006.

Address reprint requests to Akiko Furuta, M.D., Ph.D., Department of Degenerative Neurological Diseases, National Institute of Neuroscience, National Center of Neurology and Psychiatry, 4-1-1, Ogawahigashi, Kodaira, Tokyo 187-8502, Japan. E-mail: afuruta@ncnp.go.jp.

activity.[13] These mutant mice display postnatal retinal and muscular degenerations as well as mild growth retardation.[17] Retinal development is morphologically normal, but progressive retinal degeneration is reported to be evident at 3 months after birth.[17] However, precise chronological changes and the mechanism of the retinal degeneration in *Uchl3*-deficient mice has not been studied.

Both the caspase-dependent pathway and the caspase-independent pathway have been proposed to be involved in the models of retinal degeneration, including model animals for retinitis pigmentosa (such as Royal College of Surgeons (RCS) rat and retinal degeneration (*rd*) mice),[18] retinal detachment,[19] light injury,[20,21] ischemic injury,[22] and age-related macular degeneration.[23] In the ubiquitin system, UCH-L1 is involved in ischemia-induced apoptosis in the inner retina.[24] The role of UCH-L3 in retinal degeneration, however, is unclear.

To elucidate the function of UCH-L3, we investigated the histopathological changes and protein expression with respect to apoptotic pathways in *Uchl3*-deficient mice. Our results show that UCH-L3 is mainly localized to the photoreceptor inner segment that contains abundant mitochondria in the normal retina. *Uchl3*-deficient mice displayed caspase-independent apoptosis during postnatal retinal degeneration associated with increased expression of the markers for mitochondrial oxidative stress at the inner segment. We propose a possible antiapoptotic role of UCH-L3 in photoreceptor cells.

## Materials and Methods

### Animals

We used age-matched *Uchl3*-deficient mice and wild-type mice, all of which were offspring male from 15 to 20 pairs of heterozygotes that had been backcrossed with C57BL/6J at postnatal ages of 0 days (P0), 10 days (P10), 3 weeks (3w), 6 weeks (6w), 8 weeks (8w), and 12 weeks (12w). The total number of wild-type and *Uchl3*-deficient mice examined in the present study was 79, of which 30 mice were used for Western blotting, 42 mice were used for hematoxylin and eosin staining, immunohistochemistry, and terminal deoxynucleotidyl transferase-mediated dUTP nick end labeling (TUNEL) assay, and 7 mice were used for electron microscopy. The mice were maintained at the National Institute of Neuroscience, National Center of Neurology and Psychiatry (Tokyo, Japan). The experiments using the mice were approved by the Institute's Animal Investigation Committee.

### Western Blotting

Eyes from P10-, 3w-, and 6w-old mice of both genotypes (10 mice in each time point, for a total of 30 mice) were lysed in protein lysis buffer (100 mmol/L Tris-HCl, pH 8.0, 300 mmol/L NaCl, 2% Triton X-100, 0.2% SDS, 2% sodium deoxycholate, 2 mmol/L EDTA) containing protease inhibitor (Complete protease inhibitor cocktail; Sigma-Aldrich, St. Louis, MO). The amount of total protein of each sample was determined by the Bio-Rad protein assay (Bio-Rad, Hercules, CA) using bovine serum albumin as a standard. Total protein (50 $\mu$g/lane) was separated by 15% SDS-polyacrylamide gels (Perfect NT Gel, DRC, Tokyo, Japan). Proteins were transferred to immuno-Blot polyvinylidene difluoride membranes (Bio-Rad) and incubated with 5% skim milk in TBST (50 mmol/L Tris-HCl-buffered saline, pH 7.0, containing 0.05% Triton X-100) for 1 hour at room temperature. The membranes were incubated with a 1:1000 dilution of each primary antibody for UCH-L1, UCH-L3,[25] and $\beta$-actin (1:1000; Sigma-Aldrich) overnight at 4°C. For the preparation of anti-mouse UCH-L1 antibody, histidine-tagged mouse UCH-L1 (6His-mUCH-L1) was prepared as described previously[26] and used to generate a polyclonal antiserum in rabbit (Takara, Tokushima, Japan). The polyclonal antibody was purified by affinity chromatography. The specificity of this antibody to the mouse UCH-L1 was verified by Western blotting using brain lysates from *gad* mice and wild-type mice (data not shown). The membranes were washed in TBST and further incubated with antimouse or rabbit IgG-horseradish peroxidase conjugate (1:1000; Chemicon, Temecula, CA). After washing in TBST, the membranes were developed with the Super Signal West Dura or Femto Extended Duration Substrate (Pierce, Rockford, IL) and analyzed with a ChemiImager (Alpha Innotech, San Leandro, CA). Western blotting was performed five times per each antibody.

### Morphometric Analysis and Immunohistochemistry of Retina

Mice of both genotypes at P0, P10, 3w, 6w, 8w, and 12w of age (7 mice in each time point, total of 42 mice) were deeply anesthetized with diethylether, decapitated, and the eyes removed, immersion-fixed with 4% paraformaldehyde overnight at 4°C, and embedded in paraffin wax. Deparaffinized sections were stained with hematoxylin and eosin and examined under an Axioplan2 microscope (Carl Zeiss, Oberkochen, Germany) at a magnification ×400, and the thickness of each layer was measured using WinRoof software (Mitani Shoji, Tokyo, Japan).

For immunohistochemical studies, 5-$\mu$m-thick sagittal sections at the level of the optic nerve were deparaffinized and treated with 1% hydrogen peroxide ($H_2O_2$) for 30 minutes, incubated with 1% skim milk in phosphate-buffered saline (PBS, pH 7.4) for 1 hour at room temperature followed by incubation overnight at 4°C with each primary antibody for UCH-L1 and UCH-L3[25] diluted 1:500 in 1% skim milk in PBS. To characterize apoptosis- and oxidative stress-related proteins, antibodies to the following proteins were used; apoptosis-inducing factor (AIF; 1:500, Chemicon), caspase-1 (1:100; Cell Signaling Technology, Beverly, MA), caspase-3 (1:1000; Cell Signaling Technology), cleaved caspase-3 (1:50; Cell Signaling Technology), cytochrome *c* (1:1000; Santa Cruz Biotechnology, Santa Cruz, CA), cytochrome *c* oxidase I

(COX, 1:10,000; Molecular Probes, Eugene, OR), endonuclease G (Endo G; 1:500, Chemicon) and manganese superoxide dismutase (Mn-SOD; 1:10,000, Stressgen, Victoria, BC, Canada). The sections were washed in PBS and then incubated with biotinylated secondary antibodies diluted 1:500 in PBS containing 1% skim milk. The sections were treated with the VECTASTAIN Elite ABC kit (Vector Laboratories, Burlingame, CA) according to the manufacturer's protocol and developed with 0.02% 3,3′-diaminobenzidine tetrahydrochloride solution containing 0.003% $H_2O_2$. After visualization, sections were counterstained with hematoxylin. Sections were examined with an Axioplan2 microscope (Carl Zeiss). Immunohistochemistry was performed in at least three repeated experiments. The relative immunoreactivity for COX, Mn-SOD, AIF, and Endo G in each layer of mutant mice was compared with that of wild-type mice and was classified into no change (−), slight increase (±), mild increase (+), and marked increase (++).

## *TUNEL Staining*

Apoptotic cells were examined in mice of both genotypes at P0, P10, 3w, 6w, 8w, and 12w (7 mice in each time point, for a total of 42 mice) by TUNEL stain using the Dead-End Fluorimetric TUNEL system kit (Promega, Madison, WI) according to the manufacturer's instructions. The sections were examined by using a confocal laser scanning microscope (Olympus, Tokyo, Japan). The microphotographs were captured at magnification ×400 (0.066 $mm^2$/each retinal section), positive cells were counted (Fluoview 2.0; Olympus), and the data were subjected to statistical analysis.

## *Electron Microscopic Analysis*

3w-old mice of both genotypes (total 7 mice) were deeply anesthetized with 20% chloral hydrate aqueous solution and perfused with the following fixative: 2% paraformaldehyde, 2% glutaraldehyde in PBS, or sodium cacodylate buffer (pH 7.4). The eyes were removed and postfixed with the same fixative overnight at 4°C. The posterior segments of eyes were trimmed and washed with PBS or sodium cacodylate buffer, incubated in phosphate-buffered 1% osmium tetroxide for 1 hour, and dehydrated in ethanol and embedded in Epon 812 resin (TAAB, Berks, UK). Ultrathin sections (75 nm) were mounted on copper grids and stained with uranium acetate and lead citrate. The sections were observed using an H-7000 electron microscope (Hitachi, Tokyo, Japan). Morphometric analysis of mitochondria was performed by measuring average percentage of area occupied by cristae within a mitochondrion at the inner segment.

## *Statistical Analysis*

In statistical analysis of thickness of retinal layers and TUNEL-positive cells, three wild-type and four *Uchl3*-deficient mice were used in each time point (P0, P10, 3w,

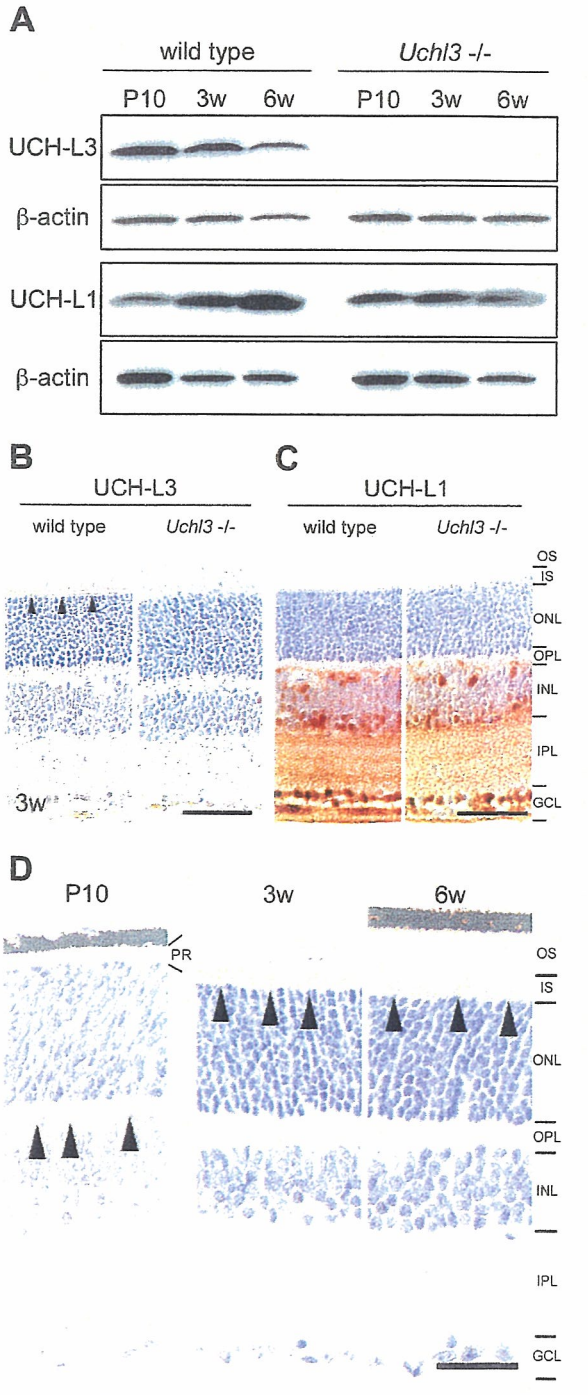


**Figure 1.** Expression of UCH-L1 and UCH-L3 in the retina of wild-type and *Uchl3*-deficient mice. **A:** Western blot analysis of UCH-L3 and UCH-L1 using whole-eye lysates from wild-type and *Uchl3*-deficient mice at P10, 3w, and 6w. The immunoreactive band for UCH-L3 is undetectable in *Uchl3*-deficient mice. Expression of UCH-L1 is similar between both genotypes. **B** and **C:** Immunohistochemistry for UCH-L3 (**B**) and UCH-L1 (**C**) in wild-type and *Uchl3*-deficient mice retinae at 3w. Immunoreactivity of UCH-L3 is found at the inner segment of the wild-type retina (**arrowheads**), whereas there is no significant immunoreactivity in *Uchl3*-deficient mice (**B**). UCH-L1 is expressed at the inner retina in both genotypes. **D:** Immunohistochemistry of UCH-L3 at P10, 3w, and 6w in wild-type retinae. UCH-L3 is faintly expressed in the outer plexiform layer at P10 (**arrowheads**). Thereafter, immunoreactivity for UCH-L3 is found in inner segment at 3w and 6w (**arrowheads**). PR, photoreceptor; OS, outer segment; IS, inner segment; ONL, outer nuclear layer; OPL, outer plexiform layer; INL, inner nuclear layer; IPL, inner plexiform layer; GCL, ganglion cell layer. Scale bars = 50 μm (**B** and **C**) and 20 μm (**D**).

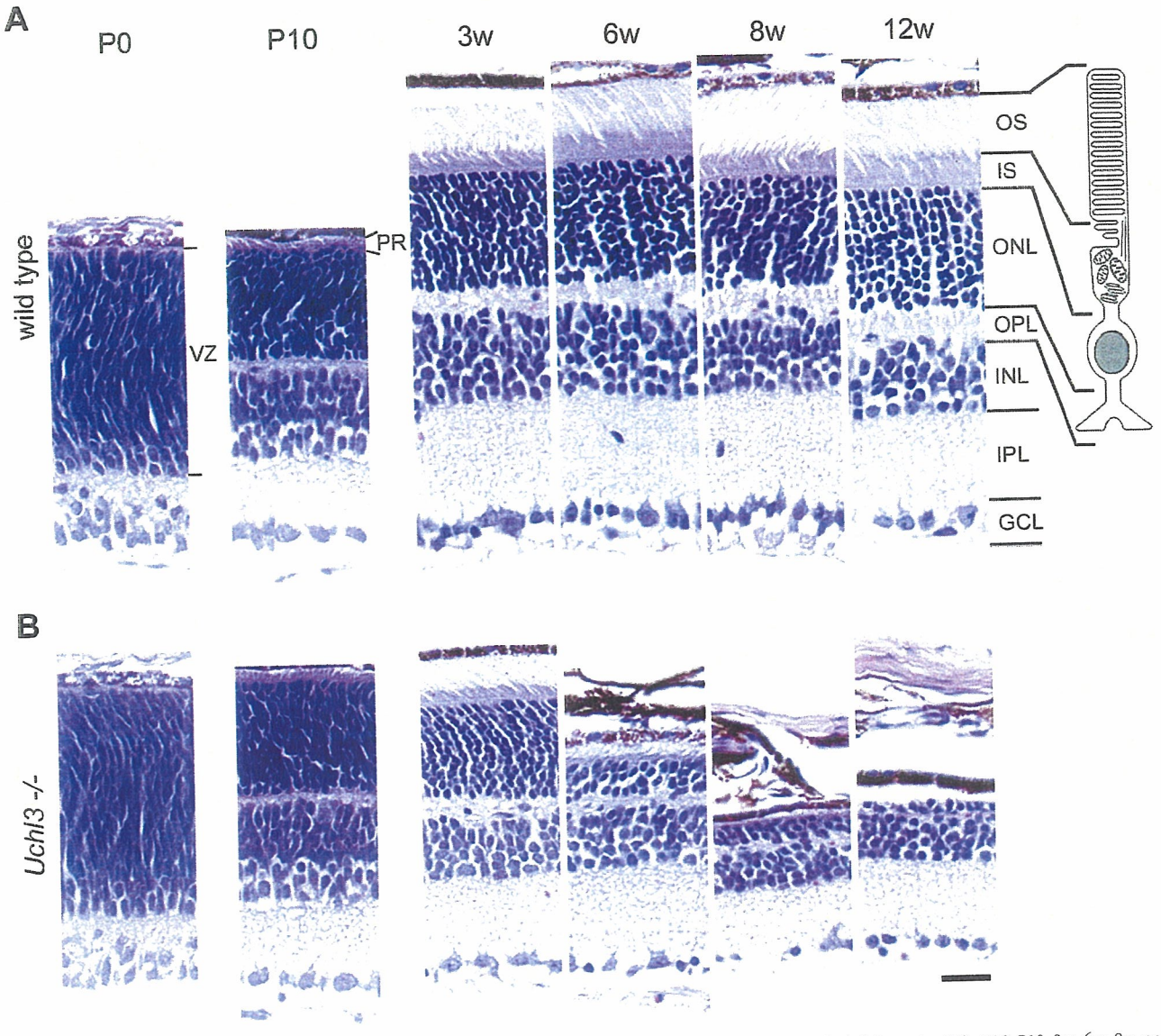


**Figure 2.** Histopathological changes of postnatal development in wild-type (**A**) and retinal degeneration of *Uchl3*-deficient mice (**B**) at P0, P10, 3w, 6w, 8w, and 12w. There is no morphological difference between both genotypes at P0 and P10, whereas outer and inner segments, outer nuclear layers, and outer plexiform layers are progressively degenerated after 3w of age. The illustration indicates a rod photoreceptor cell. VZ, ventricular zone; PR, photoreceptor; OS, outer segment; IS, inner segment; ONL, outer nuclear layer; OPL, outer plexiform layer; INL, inner nuclear layer; IPL, inner plexiform layer; GCL, ganglion cell layer. H&E staining. Scale bar = 20 μm (**A** and **B**).

6w, 8w, and 12w; for a total of 42 mice). The percentage of cristae area to whole mitochondrion in ultramicrophotographs was measured in 50 mitochondria of each genotype from three wild-type mice and four *Uchl3*-deficient mice, and the data were subjected to statistical analysis. All statistical analyses were carried out by Student's *t*-test using Microsoft Excel.

## Results

### Expression of UCH-L3 in the Murine Retina

Western blotting detected UCH-L3 (~30 kd) in extracts of eyes from wild-type mice at P10, 3w, and 6w, but the band was undetectable in *Uchl3*-deficient mice (Figure 1A). The expression level of UCH-L1 was similar in both genotypes. There was a tendency that the level of UCH-L3 decreased with age while the level of UCH-L1 increased with age in wild-type mice of all samples examined (five blots per antibody). Immunohistochemically, the cellular distribution of UCH-L3 differed from that of UCH-L1. UCH-L3 was enriched in the photoreceptor inner segment in wild-type mice at 3w of age (Figure 1B), whereas UCH-L1 was expressed in both genotypes in the inner retina, which consists of the inner nuclear layer, inner plexiform layer, and ganglion cell layer (Figure 1C). Localization of UCH-L3 in the wild-type retina was altered with age (Figure 1D). Immunoreactivity for UCH-L3 was not found at P0. UCH-L3 was faintly expressed in the outer plexiform layer at P10. Thereafter, it was localized to

inner segment at 3w. The inner segment was less immunoreactive for UCH-L3 at 6w, 8w, and 12w, compared with 3w.

## *Histopathological Changes of Retinal Degeneration in the Uchl3-Deficient Mice*

Microscopic examination of retinal cross-sections revealed no obvious histopathological changes during early postnatal development at P0 and P10 in the retina of *Uchl3*-deficient mice (Figure 2). At 3w of age, the mutant retina began to degenerate in the inner segment and ultimately disappeared at 12w (Figures 2B and 3D). Thickness of the outer segment, outer nuclear layer, and outer plexiform layer was also significantly decreased in the mutant mice at 6w of age (Figure 3, C, E, and F). Despite the conspicuous change in the photoreceptor cells, the thickness of the mutant inner retina up to 12w of age was not altered compared with that of the wild-type (Figure 3, G–I).

Ultrastructurally, vacuolar changes were found in the inner segment of *Uchl3*-deficient mice at 3w of age (Figure 4). Mitochondria at the inner segment of mutant mice were slightly swollen. Groups of small round-to-oval structures were observed in the degenerated inner segment (Figure 4D), and these structures were considered to be the cross-sections of cell processes. Chromatin condensation in photoreceptor nuclei was sometimes seen in the outer nuclear layer at 3w (Figure 4F). Morphometric analysis showed that the percentage of cristae area to whole area of mitochondrion in the inner segment of *Uchl3*-deficient mice was significantly lower than that of wild-type mice (Figure 4, G and H).

## *Altered Expressions of Apoptosis-Related Proteins in the Degenerated Retina*

Apoptotic cells in the retinal cross-sections were identified using the TUNEL staining. TUNEL-positive cells were identified in the ventricular zone at P0 and inner nuclear layer at P10 of both genotypes during the developmental period (Figure 5, A and C). The number of TUNEL-positive cells slightly increased in the inner nuclear layer at P10. After 3w of age, TUNEL-positive cells of mutant retina significantly increased at the outer nuclear layer of the mutant retina at 3w, 6w, and 8w (Figure 5, A and D).

To determine which apoptotic pathway was activated in *Uchl3*-deficient mice, we examined immunoreactivities of apoptosis-related proteins. Expression of cytochrome *c*, caspase-3, and cleaved caspase-3 and caspase-1, essential molecules for the caspase-dependent pathway, were unchanged in both genotypes (Figure 6A), whereas oxidative stress markers, COX and Mn-SOD as well as AIF and Endo G, indicators of the caspase-independent pathway, were altered in the mutant retina (Figure 6B). Chronological changes in expression of markers for oxidative stress and caspase-independent apoptosis at P0, P10, 3w, 6w, 8w, and 12w are shown in Table 1. The immunoreactivity of COX was increased in the inner segment at 3w and 6w. Mn-SOD was mildly increased in the inner segment at 3w, 6w, and 8w. Although AIF was enriched in the inner segment of *Uchl3*-deficient mice at 3w and 6w, nuclear labeling of AIF was not observed. On the other hand, Endo G was localized to the nuclei of the outer nuclear layer of the mutant retina at 3w and 6w. Expression of Endo G was slightly increased in the outer plexiform layer, inner nuclear layer, and inner plexiform layer of *Uchl3*-deficient mice after 3w of age (Table 1). Thus, degeneration of photoreceptor cells in *Uchl3*-defi-

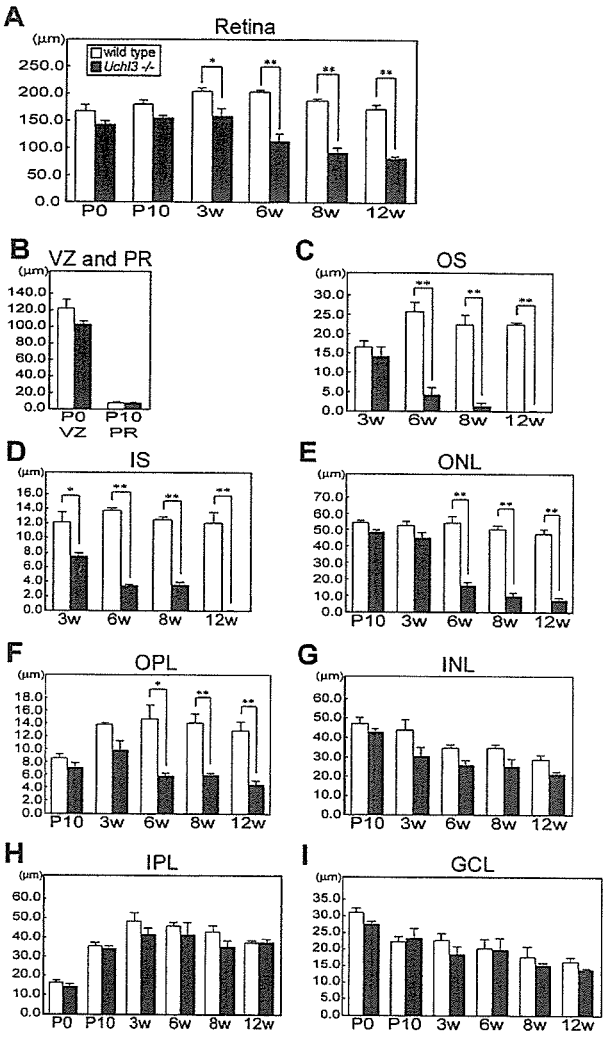


**Figure 3.** Chronological changes of retinal degeneration as assessed by thickness of each layer at different ages in wild-type and *Uchl3*-deficient mice. **A:** Total retinal thickness is progressively decreased after 3w of age. **B:** Thickness of ventricular zone at P0 and photoreceptor layer at P10 shows no significant changes between both genotypes. **C–F:** Thickness of outer retinal layers in wild-type and *Uchl3*-deficient mice at different ages. The earliest change is revealed at 3w of age in inner segment of mutant retina (**D**). Thickness of outer segment (**C**), outer nuclear layer (**E**), and outer plexiform layer (**F**) in *Uchl3*-deficient mice is significantly decreased with age compared with that in the wild-type. **G–I:** Thickness of inner retinal layers in wild-type and *Uchl3*-deficient mice at different ages. Thickness of inner nuclear layer (**G**), inner plexiform layer (**H**), and ganglion cell layer (**I**) are unchanged between both genotypes. Each value represents the mean ± SE ($^*P < 0.05$; $^{**}P < 0.01$). In all panels, the white bars represent the thickness in wild-type mice and the black bars represent the thickness in *Uchl3*-deficient mice. VZ, ventricular zone; PR, photoreceptor; OS, outer segment; IS, inner segment; ONL, outer nuclear layer; OPL, outer plexiform layer; INL, inner nuclear layer; IPL, inner plexiform layer; GCL, ganglion cell layer.

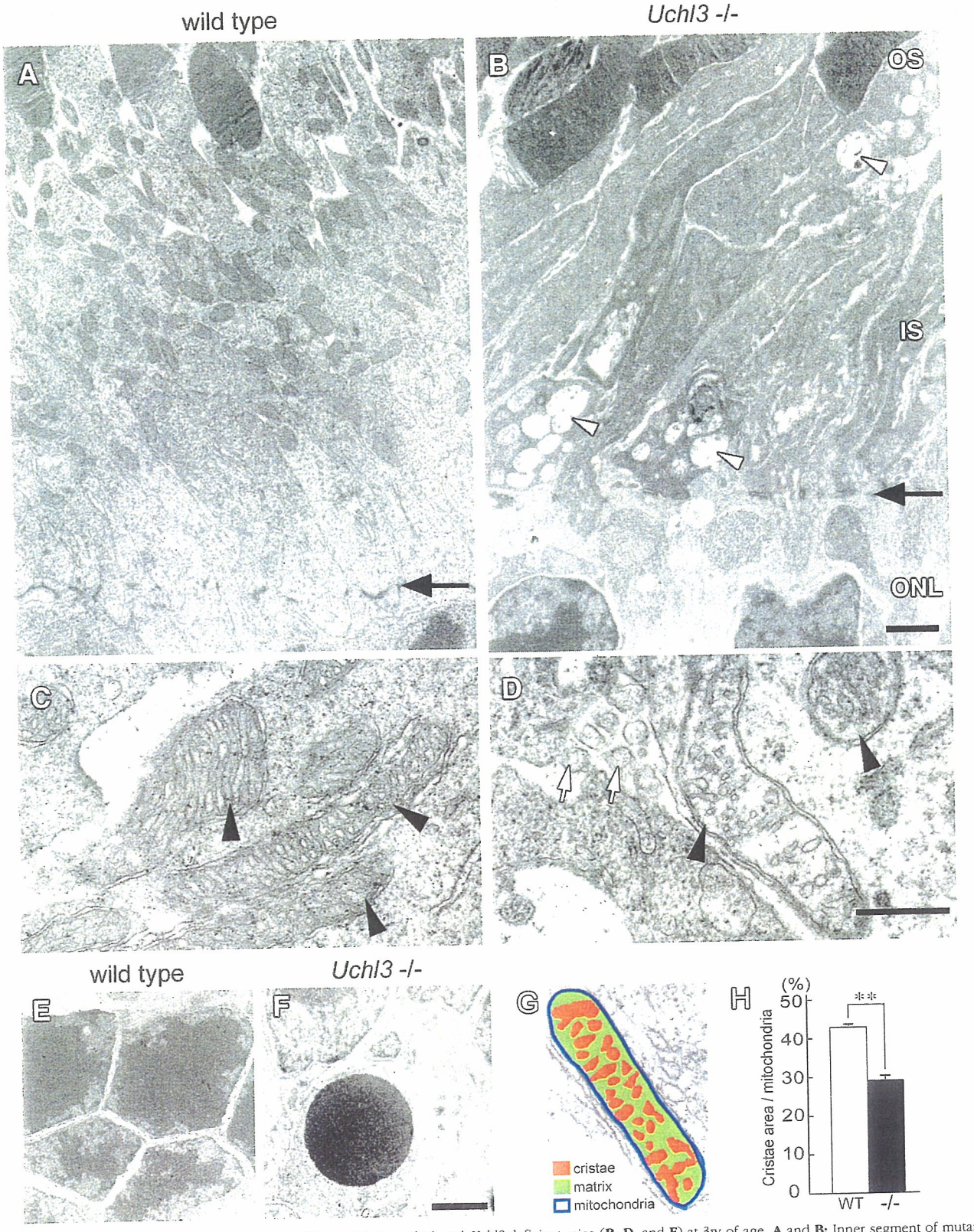


**Figure 4.** Ultrastructure of the outer retina in wild-type (**A**, **C**, and **E**) and *Uchl3*-deficient mice (**B**, **D**, and **F**) at 3w of age. **A** and **B:** Inner segment of mutant retina is shrunken associated with vacuolar changes (**arrowheads** in **B**). **Arrows** in **A** and **B** indicate outer limiting membrane. **C** and **D:** Subsets of mitochondria at the inner segment in *Uchl3*-deficient mice are swollen with decreased cristae (**arrowheads** in **D**) compared with that of wild-type (**arrowheads** in **C**). Groups of small round-to-oval shaped structures are occasionally seen in degenerated inner segment (**white arrows** in **D**). **E** and **F:** Outer nuclear layer of wild-type (**E**) and *Uchl3*-deficient (**F**) mice. Chromatin condensation of photoreceptor cells is observed in mutant mice (**F**). **G** and **H:** Morphometric analysis of mitochondria was performed with the percentage of cristae area (**G**; **red**) against mitochondrial area ($n = 50$ for each genotype). Cristae area in the inner segment is significantly decreased in mutant retina (**H**, $-/-$, **black bar**) compared with that in wild-type (**H**, WT, **white bar**). Each value represents the mean ± SE ($^{**}P < 0.01$). OS, outer segment; IS, inner segment; ONL, outer nuclear layer. Scale bars = 1 $\mu$m (**A** and **B**), 500 nm (**C** and **D**), and 1 $\mu$m (**E** and **F**).

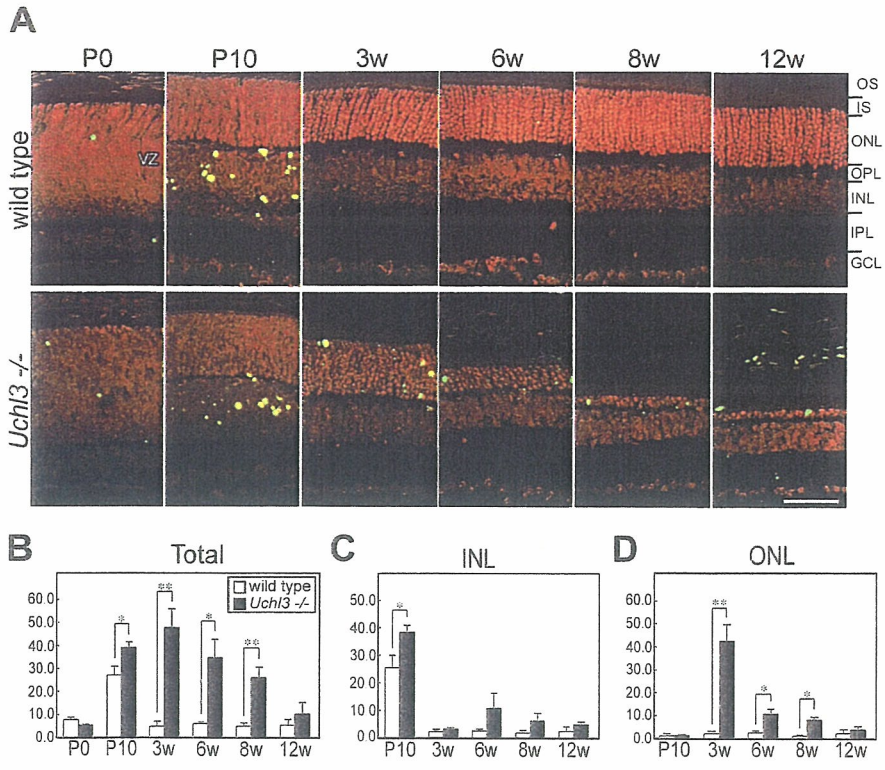


**Figure 5.** TUNEL analysis in wild-type and *Uchl3*-deficient mice at different ages. **A:** TUNEL staining in fluorescent microscopy shows that TUNEL-positive cells (**green**) are observed at the ventricular zone at P0 as well as at the inner nuclear layer at P10 in both genotypes. After 3w of age, TUNEL-positive cells are found in the outer nuclear layer in *Uchl3*-deficient mice. All sections are counterstained with propidium iodide (**red**). **B–D:** Number of TUNEL-positive cells in mutant mice (*Uchl3*$^{-/-}$; **black bar**) is significantly increased compared with those in wild-type (wild-type; **white bar**) at P10, 3w, 6w, and 8w (**B**). Increased number of TUNEL-positive cells in mutant mice at P10 correspond to apoptosis in the inner nuclear layer (**C**), whereas that in 3w, 6w, and 8w is reflected to apoptosis in the outer nuclear layer (**D**). VZ, ventricular zone; OS, outer segment; IS, inner segment; ONL, outer nuclear layer; OPL, outer plexiform layer; INL, inner nuclear layer; IPL, inner plexiform layer; GCL, ganglion cell layer. Scale bar = 20 $\mu$m (**A**). Each value in **B–D** represents the mean ± SE ($^{*}P < 0.05$; $^{**}P < 0.01$).

cient mice may be due to caspase-independent apoptotic pathway (Figure 7). Ubiquitin and Nedd-8, which are considered to be associated with UCH-L3 *in vitro*,[14,15] were expressed in the inner retina of both genotypes in a similar pattern as UCH-L1 (data not shown).

## Discussion

This study demonstrates the unique localization of UCH-L3 to the photoreceptor inner segment that is abundantly populated with mitochondria after 3w of age in wild-type mice. The following features were found with regard to retinal degeneration in *Uchl3*-deficient mice. The retina showed no obvious morphological abnormalities during early postnatal development; however, progressive retinal degeneration was observed after 3w of age. The inner segment was originally perturbated with ultrastructural changes of mitochondria and increased expressions of markers for oxidative stress. The caspase-independent pathway was implicated during photoreceptor cell apoptosis. Thus, UCH-L3 may have a role in preventing mitochondrial oxidative stress-related apoptosis in photoreceptor cells.

### Differential Localization of UCH-L1 and UCH-L3 in Murine Retina

The cellular distribution of UCH-L3 has not been studied except in the testis and epididymis, where UCH-L1 and UCH-L3 have distinct expression patterns.[25] In the present study, we found that UCH-L3 was enriched in the photoreceptor inner segment after 3w of age, whereas UCH-L1 was widely expressed in the inner retina. Photoreceptor cells are highly differentiated, and each segment has specific morphology and function; eg, inner segment contains abundant mitochondria,[27] and its oxygen consumption is considered to be high.[28] Meanwhile, expression of UCH-L1 at the inner retina was associated with that of ubiquitin and Nedd-8. Although *in vitro* studies indicate that UCH-L3 has de-neddylation activity,[14] UCH-L1 may be responsible for regulating expression level of ubiquitin and ubiquitin-like protein Nedd-8 in the retina. Because UCH-L1 expression in the retina was not altered in *Uchl3*-deficient mice, the function of UCH-L3 may not be compensated by UCH-L1. Our results indicate that UCH-L3 and UCH-L1 differ with regard to their localization and function in retina.

### Mechanism of Photoreceptor Cell Death in the Uchl3-Deficient Mice

In our result, retinal apoptosis in *Uchl3*-deficient mice consisted of two different phases, during retinal development and after development. During the early postnatal development at P10, TUNEL-positive cells were observed in the inner nuclear layer of both genotypes, and the physiological apoptosis was slightly enhanced in the mutant retina. Because UCH-L3 was faintly expressed in the outer plexiform layer at P10 in wild-type mice, UCH-L3 may function during development. In the retinal development, the number of bipolar and Müller cell deaths reaches a peak at the postnatal days 8 to 11, which is associated with differentiation of the retina in

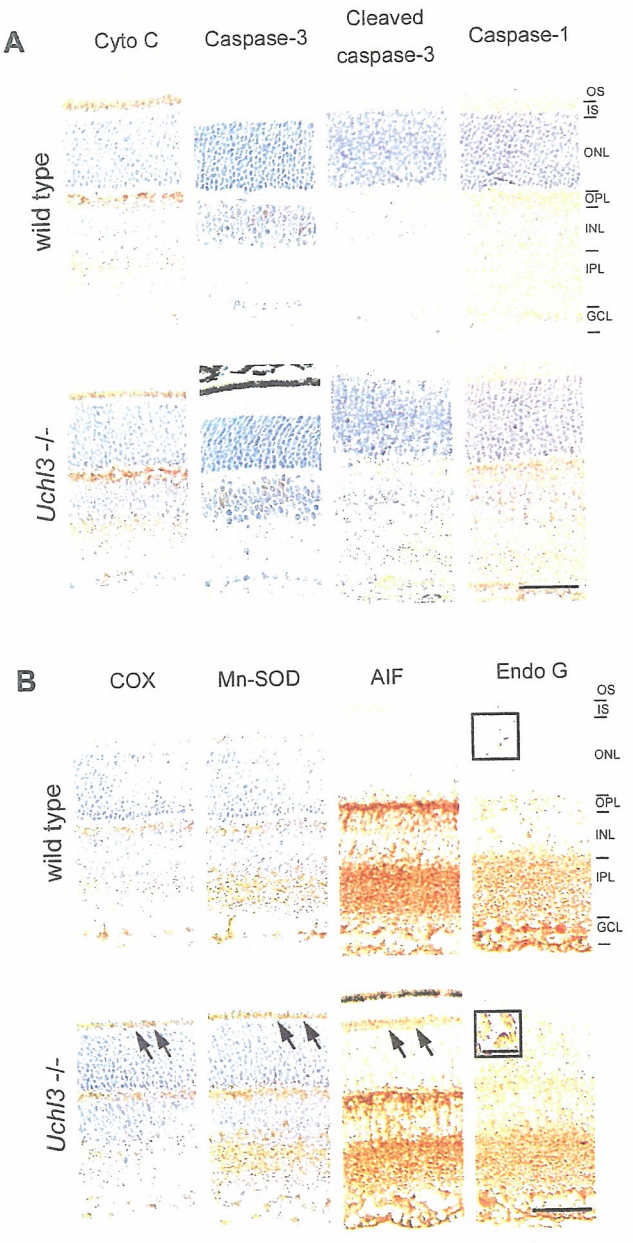


**Figure 6.** Immunohistochemical analysis of apoptosis- and oxidative stress-related molecules at 3w of age in wild-type and *Uchl3*-deficient mice. **A:** Expression of molecules relevant to the caspase-dependent pathway, including cytochrome *c* (Cyto C), caspase-3, cleaved caspase-3, and caspase-1, is unchanged between both genotypes. **B:** Increased immunoreactivities for oxidative stress markers, COX, Mn-SOD, and AIF, are observed in the inner segment of *Uchl3*-deficient mice (**arrows**). Translocation of Endo G to nuclei is found in the outer nuclear layer of *Uchl3*-deficient mice (**inset** in **B**). OS, outer segment; IS, inner segment; ONL, outer nuclear layer; OPL, outer plexiform layer; INL, inner nuclear layer; IPL, inner plexiform layer; GCL, ganglion cell layer. Scale bars = 50 μm (**A** and **B**); 10 μm (**inset** in **B**).

mice.[29] Therefore, loss of UCH-L3 may mildly promote the cell death of these cells.

After 3w of age, prominent and progressive photoreceptor cell apoptosis was disclosed in the outer nuclear layer of *Uchl3*-deficient mice. Under pathological conditions, several apoptotic pathways have been suggested in experimental retinal degeneration. Caspase-1 is predominantly associated with photoreceptor cell apoptosis in retinal degeneration of ischemia-reperfusion.[30] Light-induced retinal degeneration activates the parallel cascades, caspase-1[20] and caspase-independent apoptosis.[21] Oxidative stress leads to caspase-independent apoptosis in cultured cells.[31] Our results indicated that a caspase-independent pathway was activated during photoreceptor cell apoptosis in *Uchl3*-deficient mice, because immunohistochemical analysis revealed that activated caspase-3 and caspase-1 were not expressed in the degenerated retina. In addition, Endo G, a protein involved in the caspase-independent pathway, was expressed in the nuclei of the outer nuclear layer in *Uchl3*-deficient mice. Endo G is a mitochondria-specific nuclease that translocates to nuclei and serves as the DNase during a caspase-independent apoptosis.[32] Therefore, Endo G may be responsible for the DNA degradation that occurs during apoptosis in *Uchl3*-deficient mice. Expression of Endo G was slightly increased in the outer plexiform layer, inner nuclear layer, and inner plexiform layer of the *Uchl3*-deficient mice after 3w of age despite no significant UCH-L3 immunoreactivities in these layers. This result may reflect trans-synaptic secondary neuronal degeneration or glial changes of Müller cells.

AIF, another factor involved in caspase-independent apoptosis, was enriched in the inner segment; however, we did not observe translocation to nuclei for this protein. AIF is a mitochondrial flavoprotein that is a free radical scavenger of healthy cells.[33] During apoptotic induction, AIF translocates from mitochondria to nuclei.[33,34] It functions as a caspase-independent and PARP-1-dependent death effector that induces chromatin condensation and large-scale DNA fragmentation.[35] In our study, expression of AIF at the inner segment was associated with increased immunoreactivities of the oxidative stress markers, COX and Mn-SOD. Although it is unknown why AIF did not translocate to nuclei in the degenerated retina, increased immunoreactivity for AIF in the inner segment may indicate a reaction to oxidative stress. Because mouse eyes open 12 to 13 days after birth, light-induced oxidative stress may affect photoreceptor cell apoptosis in *Uchl3*-deficient mice after development. On the other hand, the retinal oxygen consumption increases under dark-adapted condition in the cat retina.[28,36] It may be interesting to study whether constant light or constant dark has any effect on the development of retinal degeneration in the *Uchl3*-deficient mice.

## *Uchl3*-Deficient Mice as a Model of Retinal Degeneration with Mitochondrial Impairment

Apoptosis during retinal degeneration is observed in inherited diseases such as retinitis pigmentosa as well as in retinal diseases induced by a variety of stimuli, including hypoxia and oxidative stresses.[37,38] Several genetically engineered animal models of retinitis pigmentosa have been extensively investigated, including the RCS rat and *rd* mice. Retinal degeneration in the RCS rat was originally identified as an impairment of phagocytosis by pigmented epithelium due to mutation of receptor ty-

**Table 1.** Chronological Changes in Expression of Markers for Oxidative Stress and Caspase-Independent Apoptosis

| | COX | | | | | | Mn-SOD | | | | | | AIF | | | | | | Endo G | | | | | |
|---|---|---|---|---|---|---|---|---|---|---|---|---|---|---|---|---|---|---|---|---|---|---|---|---|
| | P0 | P10 | 3w | 6w | 8w | 12w | P0 | P10 | 3w | 6w | 8w | 12w | P0 | P10 | 3w | 6w | 8w | 12w | P0 | P10 | 3w | 6w | 8w | 12w |
| VZ* | − | | | | | | − | | | | | | − | | | | | | − | | | | | |
| PR | | − | | | | | | − | | | | | | − | | | | | | − | | | | |
| OS | | | − | − | nd | nd | | | − | − | nd | nd | | | − | − | nd | nd | | | − | − | nd | nd |
| IS | | | + | + | − | nd | | | + | + | + | nd | | | ++ | + | − | nd | | | − | − | − | nd |
| ONL | | − | − | − | − | − | | − | − | − | − | − | | − | − | − | − | − | | − | ++§ | +§ | − | − |
| OPL | | − | − | − | − | − | | − | − | − | − | − | | − | − | − | − | − | | − | ± | ± | ± | ± |
| INL | | − | − | − | − | − | | − | − | − | − | − | | − | − | − | − | − | | − | ±§ | ±§ | − | − |
| IPL | − | − | − | − | − | − | − | − | − | − | − | − | − | − | − | − | − | − | − | − | − | − | ± | ± |
| GCL | − | − | − | − | − | − | − | − | − | − | − | − | − | − | − | − | − | − | − | − | − | − | − | − |

*VZ, ventricular zone; PR, photoreceptor; OS, outer segment; IS, inner segment; ONL, outer nuclear layer; OPL, outer plexiform layer; INL, inner nuclear layer; IPL, inner plexiform layer; GCL, ganglion cell layer.
−, no change; ±, slight increase; +, mild increase; and ++, marked increase of immunoreactivity compared to that of wild type.
nd, not determined due to atrophic change.
§Nuclear staining.

rosine kinase (Mertk) with subsequent photoreceptor cell death occurring in a caspase-1- and -2-dependent manner.[39–42] *rd* mice have a recessive mutation in the rod cGMP phosphodiesterase β-subunit, and photoreceptor apoptosis occurs via a caspase-dependent mechanism.[43,44] Thus, these animal models of retinitis pigmentosa differ from *Uchl3*-deficient mice with regard to the mechanism of retinal degeneration.

The relationship between retinal degeneration and mitochondrial dysfunction has not been well studied except in Harlequin mice, which contain a mutation of AIF and exhibit progressive retinal degeneration.[45] We consider that the degeneration induced in the *Uchl3*-deficient mice is associated with mitochondrial dysfunction, because mitochondria in the inner segment of mutant retina exhibited morphological changes such as decreased cristae area. *Uchl3*-deficient mice reveal not only retinal degeneration but also muscle degeneration and mild growth retardation,[17] and thus the lack of UCH-L3 may affect general organs containing abundant mitochondria. Subtypes of mitochondrial diseases, such as chronic progressive external ophthalmoplegia and Kearns-Sayre syndrome, are caused by various mitochondrial DNA deletions and observed progressive ophthalmoplegia as well as retinitis pigmentosa.[46,47] Because UCH-L3 is predicted to be involved in the maintenance of mitochondrial function, *Uchl3*-deficient mice may be a model of disease that arises from mitochondrial impairment. Further studies are necessary to clarify the molecular mechanisms underlying retinal degeneration, as well as other organs in these animals.

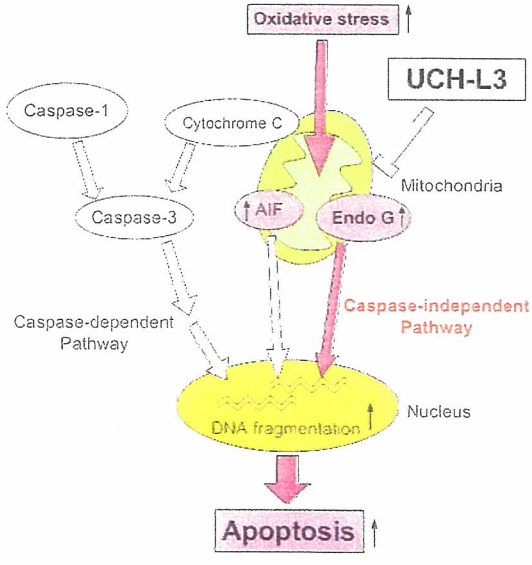


**Figure 7.** Function of UCH-L3 in apoptosis during retinal degeneration. Mitochondrial apoptosis is classified into caspase-dependent and caspase-independent pathways. Loss of UCH-L3 leads to oxidative stress-induced mitochondrial damage that causes translocation of Endo G from mitochondria to nuclei, resulting in caspase-independent apoptosis. **Red arrows** are considered to be activated in *Uchl3*-deficient mice.

## Acknowledgments

We thank Dr. S.M. Tilghman for providing *Uchl3*-deficient mice, Dr. K. Oyanagi, Dr. T. Harada, and Dr. K. Arima for their useful discussions, Ms. H. Fujita and Mr. D. Yamada for the breeding and care of the mice, and Mr. R. Debold, Ms. T. Matsuzawa, and Mr. N. Takagaki for editing the manuscript.

## References

1. Amerik AY, Hochstrasser M: Mechanism and function of deubiquitinating enzymes. Biochim Biophys Acta 2004, 1695:189–207
2. Weissman AM: Themes and variations on ubiquitylation. Nat Rev Mol Cell Biol 2001, 2:169–178
3. Pickart CM, Eddins MJ: Ubiquitin: structures, functions, mechanisms. Biochim Biophys Acta 2004, 1695:55–72
4. Aguilar RC, Wendland B: Ubiquitin: not just for proteasomes anymore. Curr Opin Cell Biol 2003, 15:184–190
5. Wilkinson KD: Regulation of ubiquitin-dependent processes by deubiquitinating enzymes. FASEB J 1997, 11:1245–1256
6. Doran JF, Jackson P, Kynoch PA, Thompson RJ: Isolation of PGP 9.5, a new human neurone-specific protein detected by high-resolution two-dimensional electrophoresis. J Neurochem 1983, 40:1542–1547
7. Wilkinson KD, Lee KM, Deshpande S, Duerksen-Hughes P, Boss JM, Pohl J: The neuron-specific protein PGP 9.5 is a ubiquitin carboxyl-terminal hydrolase. Science 1989, 246:670–673
8. Osawa Y, Wang YL, Osaka H, Aoki S, Wada K: Cloning, expression, and mapping of a mouse gene, Uchl4, highly homologous to human and mouse Uchl3. Biochem Biophys Res Commun 2001, 283:627–633

9. Liu Y, Fallon L, Lashuel HA, Liu Z, Lansbury PT Jr,: The UCH-L1 gene encodes two opposing enzymatic activities that affect alpha-synuclein degradation and Parkinson's disease susceptibility. Cell 2002, 111:209–218
10. Leroy E, Boyer R, Auburger G, Leube B, Ulm G, Mezey E, Harta G, Brownstein MJ, Jonnalagada S, Chernova T, Dehejia A, Lavedan C, Gasser T, Steinbach PJ, Wilkinson KD, Polymeropoulos MH: The ubiquitin pathway in Parkinson's disease. Nature 1998, 395:451–452
11. Saigoh K, Wang YL, Suh JG, Yamanishi T, Sakai Y, Kiyosawa H, Harada T, Ichihara N, Wakana S, Kikuchi T, Wada K: Intragenic deletion in the gene encoding ubiquitin carboxy-terminal hydrolase in *gad* mice. Nat Genet 1999, 23:47–51
12. Wilkinson KD, Deshpande S, Larsen CN: Comparisons of neuronal (PGP 9.5) and non-neuronal ubiquitin C-terminal hydrolases. Biochem Soc Trans 1992, 20:631–637
13. Kurihara LJ, Semenova E, Levorse JM, Tilghman SM: Expression and functional analysis of *Uch-L3* during mouse development. Mol Cell Biol 2000, 20:2498–2504
14. Wada H, Kito K, Caskey LS, Yeh ET, Kamitani T: Cleavage of the C-terminus of NEDD8 by UCH-L3. Biochem Biophys Res Commun 1998, 251:688–692
15. Gan-Erdene T, Nagamalleswari K, Yin L, Wu K, Pan ZQ, Wilkinson KD: Identification and characterization of DEN1, a deneddylase of the ULP family. J Biol Chem 2003, 278:28892–28900
16. Kwon J, Wang YL, Setsuie R, Sekiguchi S, Sato Y, Sakurai M, Noda M, Aoki S, Yoshikawa Y, Wada K: Two closely related ubiquitin C-terminal hydrolase isozymes function as reciprocal modulators of germ cell apoptosis in cryptorchid testis. Am J Pathol 2004, 165:1367–1374
17. Semenova E, Wang X, Jablonski MM, Levorse J, Tilghman SM: An engineered 800 kilobase deletion of *Uchl3* and *Lmo7* on mouse chromosome 14 causes defects in viability, postnatal growth and degeneration of muscle and retina. Hum Mol Genet 2003, 12:1301–1312
18. Chang GQ, Hao Y, Wong F: Apoptosis: final common pathway of photoreceptor death in rd, rds, and rhodopsin mutant mice. Neuron 1993, 11:595–605
19. Cook B, Lewis GP, Fisher SK, Adler R: Apoptotic photoreceptor degeneration in experimental retinal detachment. Invest Ophthalmol Vis Sci 1995, 36:990–996
20. Grimm C, Wenzel A, Hafezi F, Remè CE: Gene expression in the mouse retina: the effect of damaging light. Mol Vis 2000, 6:252–260
21. Donovan M, Cotter TG: Caspase-independent photoreceptor apoptosis in vivo and differential expression of apoptotic protease activating factor-1 and caspase-3 during retinal development. Cell Death Differ 2002, 9:1220–1231
22. Osborne NN, Melena J, Chidlow G, Wood JP: A hypothesis to explain ganglion cell death caused by vascular insults at the optic nerve head: possible implication for the treatment of glaucoma. Br J Ophthalmol 2001, 85:1252–1259
23. Adler R, Curcio C, Hicks D, Price D, Wong F: Cell death in age-related macular degeneration. Mol Vis 1999, 5:31
24. Harada T, Harada C, Wang YL, Osaka H, Amanai K, Tanaka K, Takizawa S, Setsuie R, Sakurai M, Sato Y, Noda M, Wada K: Role of ubiquitin carboxy terminal hydrolase-L1 in neural cell apoptosis induced by ischemic retinal injury in vivo. Am J Pathol 2004, 164:59–64
25. Kwon J, Wang YL, Setsuie R, Sekiguchi S, Sakurai M, Sato Y, Lee WW, Ishii Y, Kyuwa S, Noda M, Wada K, Yoshikawa Y: Developmental regulation of ubiquitin C-terminal hydrolase isozyme expression during spermatogenesis in mice. Biol Reprod 2004, 71:515–521
26. Osaka H, Wang YL, Takada K, Takizawa S, Setsuie R, Li H, Sato Y, Nishikawa K, Sun YJ, Sakurai M, Harada T, Hara Y, Kimura I, Chiba S, Namikawa K, Kiyama H, Noda M, Aoki S, Wada K: Ubiquitin carboxy-terminal hydrolase L1 binds to and stabilizes monoubiquitin in neuron. Hum Mol Genet 2003, 12:1945–1958
27. De Robertis E: Electron microscope observations on the submicroscopic organization of the retinal rods. J Biophys Biochem Cytol 1956, 2:319–330
28. Linsenmeier RA, Braun RD: Oxygen distribution and consumption in the cat retina during normoxia and hypoxemia. J Gen Physiol 1992, 99:177–197
29. Young RW: Cell death during differentiation of the retina in the mouse. J Comp Neurol 1984, 229:362–373
30. Katai N, Yoshimura N: Apoptotic retinal neuronal death by ischemia-reperfusion is executed by two distinct caspase family proteases. Invest Ophthalmol Vis Sci 1999, 40:2697–2705
31. Carmody RJ, Cotter TG: Oxidative stress induces caspase-independent retinal apoptosis in vitro. Cell Death Differ 2000, 7:282–291
32. Li LY, Luo X, Wang X: Endonuclease G is an apoptotic DNase when released from mitochondria. Nature 2001, 412:95–99
33. Susin SA, Lorenzo HK, Zamzami N, Marzo I, Snow BE, Brothers GM, Mangion J, Jacotot E, Costantini P, Loeffler M, Larochette N, Goodlett DR, Aebersold R, Siderovski DP, Penninger JM, Kroemer G: Molecular characterization of mitochondrial apoptosis-inducing factor. Nature 1999, 397:441–446
34. Lorenzo HK, Susin SA, Penninger J, Kroemer G: Apoptosis inducing factor (AIF): a phylogenetically old, caspase-independent effector of cell death. Cell Death Differ 1999, 6:516–524
35. Yu SW, Wang H, Poitras MF, Coombs C, Bowers WJ, Federoff HJ, Poirier GG, Dawson TM, Dawson VL: Mediation of poly(ADP-ribose) polymerase-1-dependent cell death by apoptosis-inducing factor. Science 2002, 297:259–263
36. Linsenmeier RA: Effects of light and darkness on oxygen distribution and consumption in the cat retina. J Gen Physiol 1986, 88:521–542
37. Pacione LR, Szego MJ, Ikeda S, Nishina PM, McInnes RR: Progress toward understanding the genetic and biochemical mechanisms of inherited photoreceptor degenerations. Annu Rev Neurosci 2003, 26:657–700
38. Phelan JK, Bok D: A brief review of retinitis pigmentosa and the identified retinitis pigmentosa genes. Mol Vis 2000, 6:116–124
39. D'Cruz PM, Yasumura D, Weir J, Matthes MT, Abderrahim H, LaVail MM, Vollrath D: Mutation of the receptor tyrosine kinase gene Mertk in the retinal dystrophic RCS rat. Hum Mol Genet 2000, 9:645–651
40. Feng W, Yasumura D, Matthes MT, LaVail MM, Vollrath D: Mertk triggers uptake of photoreceptor outer segments during phagocytosis by cultured retinal pigment epithelial cells. J Biol Chem 2002, 277:17016–17022
41. Katai N, Kikuchi T, Shibuki H, Kuroiwa S, Arai J, Kurokawa T, Yoshimura N: Caspase-like proteases activated in apoptotic photoreceptors of Royal College of Surgeons rats. Invest Ophthalmol Vis Sci 1999, 40:1802–1807
42. Vollrath D, Feng W, Duncan JL, Yasumura D, D'Cruz PM, Chappelow A, Matthes MT, Kay MA, LaVail MM: Correction of the retinal dystrophy phenotype of the RCS rat by viral gene transfer of Mertk. Proc Natl Acad Sci USA 2001, 98:12584–12589
43. Jomary C, Neal MJ, Jones SE: Characterization of cell death pathways in murine retinal neurodegeneration implicates cytochrome c release, caspase activation, and bid cleavage. Mol Cell Neurosci 2001, 18:335–346
44. Lem J, Flannery JG, Li T, Applebury ML, Farber DB, Simon MI: Retinal degeneration is rescued in transgenic rd mice by expression of the cGMP phosphodiesterase $\beta$ subunit. Proc Natl Acad Sci USA 1992, 89:4422–4426
45. Klein JA, Longo-Guess CM, Rossmann MP, Seburn KL, Hurd RE, Frankel WN, Bronson RT, Ackerman SL: The harlequin mouse mutation downregulates apoptosis-inducing factor. Nature 2002, 419:367–374
46. Land JM, Morgan-Hughes JA, Hargreaves I, Heales SJ: Mitochondrial disease: a historical, biochemical, and London perspective. Neurochem Res 2004, 29:483–491
47. Schmiedel J, Jackson S, Schäfer J, Reichmann H: Mitochondrial cytopathies. J Neurol 2003, 250:267–277

THE JOURNAL OF BIOLOGICAL CHEMISTRY VOL. 281, NO. 41, pp. 30524–30533, October 13, 2006


# Degradation of Amyotrophic Lateral Sclerosis-linked Mutant Cu,Zn-Superoxide Dismutase Proteins by Macroautophagy and the Proteasome*[S]

Received for publication, April 7, 2006, and in revised form, August 18, 2006 Published, JBC Papers in Press, August 18, 2006, DOI 10.1074/jbc.M603337200

**Tomohiro Kabuta, Yasuyuki Suzuki, and Keiji Wada**[1]

*From the Department of Degenerative Neurological Diseases, National Institute of Neuroscience, National Center of Neurology and Psychiatry, Kodaira, Tokyo 187-8502, Japan*

**Mutations in the Cu,Zn-superoxide dismutase (SOD1) gene cause ~20% of familial cases of amyotrophic lateral sclerosis (fALS). Accumulating evidence indicates that a gain of toxic function of mutant SOD1 proteins is the cause of the disease. It has also been shown that the ubiquitin-proteasome pathway plays a role in the clearance and toxicity of mutant SOD1. In this study, we investigated the degradation pathways of wild-type and mutant SOD1 in neuronal and nonneuronal cells. We provide here the first evidence that wild-type and mutant SOD1 are degraded by macroautophagy as well as by the proteasome. Based on experiments with inhibitors of these degradation pathways, the contribution of macroautophagy to mutant SOD1 clearance is comparable with that of the proteasome pathway. Using assays that measure cell viability and cell death, we observed that under conditions where expression of mutant SOD1 alone does not induce toxicity, macroautophagy inhibition induced mutant SOD1-mediated cell death, indicating that macroautophagy reduces the toxicity of mutant SOD1 proteins. We therefore propose that both macroautophagy and the proteasome are important for the reduction of mutant SOD1-mediated neurotoxicity in fALS. Inhibition of macroautophagy also increased SOD1 levels in detergent-soluble and -insoluble fractions, suggesting that both detergent-soluble and -insoluble SOD1 are degraded by macroautophagy. These findings may provide further insights into the mechanisms of pathogenesis of fALS.**

Amyotrophic lateral sclerosis (ALS)[2] is a neurodegenerative disease caused by selective loss of motor neurons (1, 2). Although most cases of ALS are sporadic, ~10% of ALS cases run in families. Dominant missense mutations in the gene that encodes the Cu,Zn-superoxide dismutase (SOD1) are responsible for 20% of familial ALS (fALS) cases (3). Mice overexpressing mutant SOD1 develop an ALS-like phenotype comparable with human ALS, whereas mice lacking SOD1 do not (4, 5). These findings have led to the conclusion that SOD1 mutants cause motor neuron degeneration by a toxic gain of function. Thus, studies of the degradation process of mutant SOD1 proteins could provide important insights into understanding the mechanisms that underlie the pathology of fALS, and possibly sporadic ALS, and into developing novel therapies for fALS by removing toxic species of mutant SOD1.

Cytoplasmic proteins are mainly degraded by two pathways, the ubiquitin-26 S proteasome pathway (6) and autophagy (7). Previous studies have shown that mutant SOD1 proteins are turned over more rapidly than wild-type SOD1, and a proteasome inhibitor increases the level of mutant SOD1 proteins (8, 9). Dorfin and NEDL1, two distinct ubiquitin ligases, ubiquitinate mutant but not wild-type SOD1 (10, 11). These observations suggest that mutant SOD1 is degraded by the ubiquitin-26 S proteasome pathway and that the increased turnover of mutant SOD1 is mediated in part by this pathway. On the other hand, the 20 S proteasome, a component of the 26 S proteasome, can degrade proteins without a requirement for ubiquitination (12, 13). A recent study has found that metal-free forms of wild-type and mutant SOD1 are degraded by the 20 S proteasome *in vitro* (14).

Autophagy is an intracellular process that results in the degradation of cytoplasmic components inside lysosomes. At least three forms of autophagy have been described in mammalian cells: macroautophagy, microautophagy, and chaperone-mediated autophagy (7). Macroautophagy is the major and the most well studied form of autophagy; this process begins with a sequestration step, in which cytosolic components are engulfed by a membrane sac called the isolation membrane. This membrane results in a double membrane structure called the autophagosome, which fuses with the lysosome. The inner membrane of the autophagosome and its protein and organelle contents are degraded by lysosomal hydrolases. Recent reports have demonstrated that macroautophagy plays an important role in preventing neurodegeneration in mice (15, 16). Although macroautophagy can be induced by starvation, this

* This work was supported by grants-in-aid for scientific research from the Japan Society for the Promotion of Science; a research grant in a priority area of research from the Ministry of Education, Culture, Sports, Science, and Technology, Japan; grants-in-aid for scientific research from the Ministry of Health, Labor and Welfare, Japan; and the Program for Promotion of Fundamental Studies in Health Sciences of the National Institute of Biomedical Innovation, Japan. The costs of publication of this article were defrayed in part by the payment of page charges. This article must therefore be hereby marked "*advertisement*" in accordance with 18 U.S.C. Section 1734 solely to indicate this fact.

[S] The on-line version of this article (available at http://www.jbc.org) contains supplemental Figs. S1–S6.

[1] To whom correspondence should be addressed: Dept. of Degenerative Neurological Diseases, National Institute of Neuroscience, National Center of Neurology and Psychiatry, 4-1-1 Ogawahigashi, Kodaira, Tokyo 187-8502, Japan. Tel.: 81-42-346-1715; Fax: 81-42-346-1745; E-mail: wada@ncnp.go.jp.

[2] The abbreviations used are: ALS, amyotrophic lateral sclerosis; fALS, familial ALS; SOD1, Cu,Zn-superoxide dismutase(s); 3-MA, 3-methyladenine; siRNA, short interfering RNA; EGFP, enhanced green fluorescent protein; HA, hemagglutinin; MTS, 3-(4,5-dimethylthiazol-2-yl)-5-(3-carboxymethoxyphenyl)-2-(4-sulfophenyl)-2H-tetrazolium.